(1)

PENNSTATE

Using Nonequilibrium Alloying Techniques for Corrosion Inhibition in Gr/Al and Gr/Mg Metal Matrix Composites

Annual Report
June 1994

Submitted to
Office of Naval Research
800 North Quincy Street
Arlington, VA 22217-5000

Submitted by:

B.A. Shaw[1], W.C. Moshier[2], R.G. Wendt[2], P.L. Miller[1], A.E. Krebs[1], and D.J. Ciscon[1]

[1]Penn State University, University Park, PA 16802

[2]Martin Marietta Astronautics, Denver, CO 80201

SECURITY CLASSIFICATION OF THIS PAGE

REPORT DOCUMENTATION PAGE

Form Approved OMB No. 0704-0188

1a. REPORT SECURITY CLASSIFICATION: Unclassified	1b. RESTRICTIVE MARKINGS: None
2a. SECURITY CLASSIFICATION AUTHORITY	3. DISTRIBUTION/AVAILABILITY OF REPORT: Unrestricted
2b. DECLASSIFICATION/DOWNGRADING SCHEDULE	
4. PERFORMING ORGANIZATION REPORT NUMBER(S)	5. MONITORING ORGANIZATION REPORT NUMBER(S)
6a. NAME OF PERFORMING ORGANIZATION: Penn State University; 6b. OFFICE SYMBOL (If applicable): Code 1131M	7a. NAME OF MONITORING ORGANIZATION
6c. ADDRESS (City, State, and ZIP Code): Dept. of Engineering Science and Mechanics, 227 Hammond Bldg., University Park, PA 16802	7b. ADDRESS (City, State, and ZIP Code)
8a. NAME OF FUNDING/SPONSORING ORGANIZATION: Office of Naval Research; 8b. OFFICE SYMBOL (If applicable): Code	9. PROCUREMENT INSTRUMENT IDENTIFICATION NUMBER
8c. ADDRESS (City, State, and ZIP Code): 800 North Quincy St., Arlington, VA 22217-5000	10. SOURCE OF FUNDING NUMBERS: PROGRAM ELEMENT NO.; PROJECT NO. N00014-91-J-1196; TASK NO.; WORK UNIT ACCESSION NO.

11. TITLE (Include Security Classification)

Using Nonequilibrium Alloying Techniques for Corrosion Inhibition in Gr/Al and Gr/Mg Metal Matrix Composites.

12. PERSONAL AUTHOR(S)

B.A. Shaw, W.C. Moshier, R.G. Wendt, P.L. Miller, A.E. Krebs, and D.J. Ciscon

13a. TYPE OF REPORT	13b. TIME COVERED	14. DATE OF REPORT (Year, Month, Day)	15. PAGE COUNT
Technical	FROM 4/1/93 TO 3/31/94	June 15, 1994	68

16. SUPPLEMENTARY NOTATION

17. COSATI CODES			18. SUBJECT TERMS (Continue on reverse if necessary and identify by block number)
FIELD	GROUP	SUB-GROUP	Metal Matrix Composites, Gr/Al Composites, Gr/Mg Composites Nonequilibrium Alloying, Corrosion Resistance

19. ABSTRACT (Continue on reverse if necessary and identify by block number)

Metal matrix composites (MMCs) have been heavily studied over the past thirty years. During that period, many proposals have been made to develop a matrix alloy that was compatible with the reinforcing phase. However, for one reason or another, the technology has continued to focus on conventional alloys and fabrication practices. Although tremendous advances have been made on composite materials, the basic technology remains similar to systems studied twenty years ago. This work represents the first new program where new alloys are being developed for graphite reinforced composites which are tailored to a novel processing technology for manufacturing corrosion resistant graphite reinforced composites.

20. DISTRIBUTION/AVAILABILITY OF ABSTRACT	21. ABSTRACT SECURITY CLASSIFICATION
☒ UNCLASSIFIED/UNLIMITED ☐ SAME AS RPT. ☐ DTIC USERS	
22a. NAME OF RESPONSIBLE INDIVIDUAL: B.A. Shaw	22b. TELEPHONE (Include Area Code): (814) 865-7828; 22c. OFFICE SYMBOL

DD Form 1473, JUN 86 *Previous editions are obsolete.* SECURITY CLASSIFICATION OF THIS PAGE

PENNSTATE

Using Nonequilibrium Alloying Techniques for Corrosion Inhibition in Gr/Al and Gr/Mg Metal Matrix Composites

Annual Report
June 1994

Submitted to
Office of Naval Research
800 North Quincy Street
Arlington, VA 22217-5000

Submitted by:

B.A. Shaw[1], W.C. Moshier[2], R.G. Wendt[2], P.L. Miller[1], A.E. Krebs[1], and D.J. Ciscon[1]

[1]Penn State University, University Park, PA 16802

[2]Martin Marietta Astronautics, Denver, CO 80201

Table of Contents

Introduction 1

Significant Results to Date 2
- Nonequilibrium Alloys 2
- Al-Mo 2
- Al-Ti 14
- Graphite Fiber Coating 18
- Fiber Consolidation 25
- Nonequilibrium Mg Alloys 25
- Inhibitive Surface Treatments 33

Summary 37

References 38

Appendix 1 - Technical Note: Improving Corrosion Resistance of Magnesium by Nonequilibrium Alloying with Yttrium 39

Appendix 2 - Corrosion Resistant Aluminum Matrix for Graphite-Aluminum Composites 44

Introduction

High modulus graphite (Gr) reinforced metal matrix composites (MMCs) offer a wide variety of attractive properties including: high specific modulus and strength (E/ρ and UTS/ρ), tailorable or zero coefficient of thermal expansion (CTE), and high thermal conductivity. Using either Al or Mg as the matrix metal results in a reduction of the final density of the composite with high elastic modulus and excellent strength in the fiber direction. Unfortunately, MMCs, especially Gr reinforced composites, are extremely susceptible to corrosion with severe attack in chloride-containing environments occurring in as little time as several weeks for the Gr/Al composites[1-3] or in just a few days for Gr/Mg composites.[4,5]

The overall objective of this research program is to determine whether improving the inherent passivity of the matrix metal in a Gr/Al or Gr/Mg composite can alleviate, or at least minimize, galvanic corrosion between the graphite and the matrix metal. This galvanic corrosion is currently one of the limiting factors in utilization of these composites. The program focuses on the unique properties of sputter deposited alloys. With sputter deposition it is possible to significantly increase the solubility of passivity enhancing species in both Al and Mg, thus dramatically improving their corrosion resistance.[6-10] The approach that is being undertaken is to develop alloy systems capable of minimizing galvanic degradation of the composite. An essential step in this process is identification of alloy compositions which maintain enhanced passivity after processing into the bulk composite. Once these compositions have been identified, then the sputter coated fibers can be consolidated into a net-shape composite by hot isostatic pressing. This research will ultimately lead to the fabrication of a prototype filament-wound mirror support for a staring telescope.

This research addresses the following specific issues.

1) Can the passivity of Al be enhanced through nonequilibrium alloying?

2) Can the passivity of Mg be improved through nonequilibrium alloying or through the use of a cerium or yttrium based inhibitive treatment?

3) Will these passivity enhanced alloys be compatible with graphite?

4) What are the processing conditions that must be used to make a structure with these materials and still retain the enhanced corrosion performance of the alloys?

5) Can a composite structure (i.e., fiber coating, filament winding, and consolidation via hot press or hot isostatic press) with improved corrosion performance be fabricated using a nonequilibrium alloy as the matrix?

This year's report summarizes the results obtained for questions 1 through 4 above. The last year of the program will concentrate on question 5.

Significant Results to Date

Nonequilibrium Al Alloys

In our initial investigation into the use of nonequilibrium alloying for enhancing the corrosion resistance of graphite-reinforced MMCs, a variety of different nonequilibrium Al alloys (Al-Cr, Al-Mo, Al-Ta, and Al-W) were fabricated, heat-treated, and examined using x-ray diffraction (XRD), scanning electron microscopy (SEM), scanning laser microscopy (SLM), and electrochemical techniques. Based on the results of the electrochemical tests and thermal studies, Al-26W, Al-19Mo, and Al-2Mg-17W (all percentages given in this report are in atomic percent) were chosen to optimize corrosion resistance and minimize alloy density. These alloys were sputter-deposited on silicon and graphite substrates and heat-treated. Again, XRD and electrochemical corrosion assessment were conducted. XRD results indicated that all three alloys were amorphous and no evidence of alloy degradation was observed as a result of heat treatment. Anodic polarization behavior for all three alloys (Figure 1) in 0.1 M Cl^- (pH 8) was significantly enhanced when compared to that of pure Al. The Al-26W and Al-19Mo alloys were also galvanically coupled to P75 Gr for 7 days to determine whether these alloys could be used as the matrix material of a graphite reinforced MMC. Both alloys performed excellently, exhibiting coupled currents less than 0.1 μA (corresponding to 0.3 $\mu A/cm^2$ for Al-19Mo and 0.1 $\mu A/cm^2$ for Al-26W) and no degradation of the alloy surfaces. Details of these tests can be found in the April, 1992 Annual Report to ONR entitled "Inhibiting Corrosion in Gr/Al and Gr/Mg Metal Matrix Composites Using Nonequilibrium Alloying Techniques."

Al-Mo

Since all three alloys exhibited satisfactory corrosion resistance, the Al-Mo system was selected for more detailed studies of its corrosion resistance and thermal stability. Anodic and cathodic potentiodynamic polarization and long-term galvanic testing were conducted to evaluate corrosion resistance, while transmission electron microscopy (TEM) and XRD were performed to evaluate thermal stability.

Figure 2 shows representative anodic polarization curves for the binary Al-Mo and ternary Al-Mg-Mo non-equilibrium alloys in the as-sputtered condition. All as-sputtered Al-Mo alloys exhibited a passive region and an open circuit potential (E_{corr}) that was several hundred millivolts more noble than pure Al. E_{corr} values for all of the alloys were between -600 to -450 mV_{SCE} with the majority of the measured E_{corr} values ranging from -520 mV_{SCE} to -580 mV_{SCE}. There was no apparent trend in E_{corr} as a function of solute concentration for the Al-Mo alloys tested. Breakdown potential (E_b) values for most of the as-sputtered alloys were between 100 and 500 mV_{SCE} as compared to -690 mV_{SCE} for pure Al. Passive current densities (i_{pass}) for the as-deposited binary Al-Mo and ternary Al-Mg-Mo alloys ranged between 0.1 and 1.0 $\mu A/cm^2$, but as in the case of E_{corr}, no correlation between solute concentration and i_{pass} was

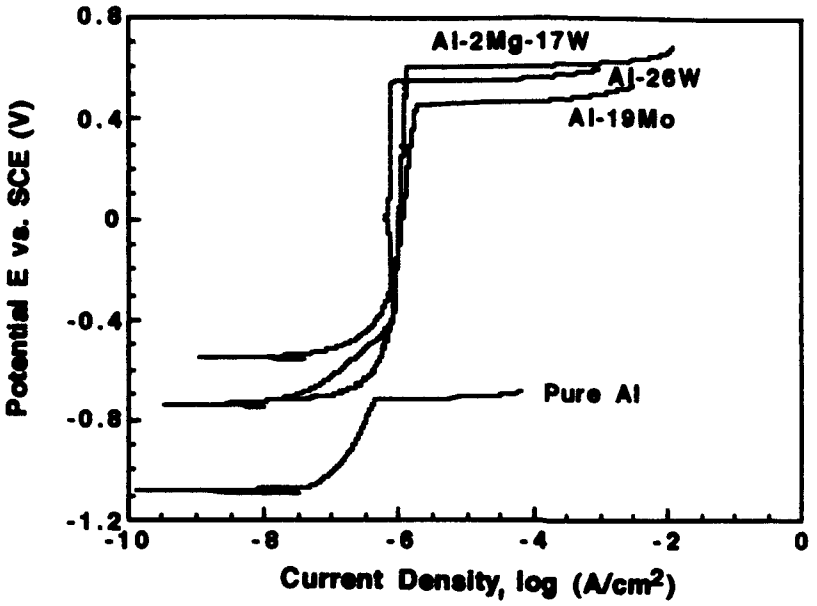

Figure 1. *Anodic Polarization Behavior of Al-26W, Al-19Mo and Al-2Mg-17W Compared to Pure Aluminum, all Deposited on Si. Tests Were Generated at a Scan Rate of 0.2 mV/s in 0.1 M NaCl (pH = 8) .*

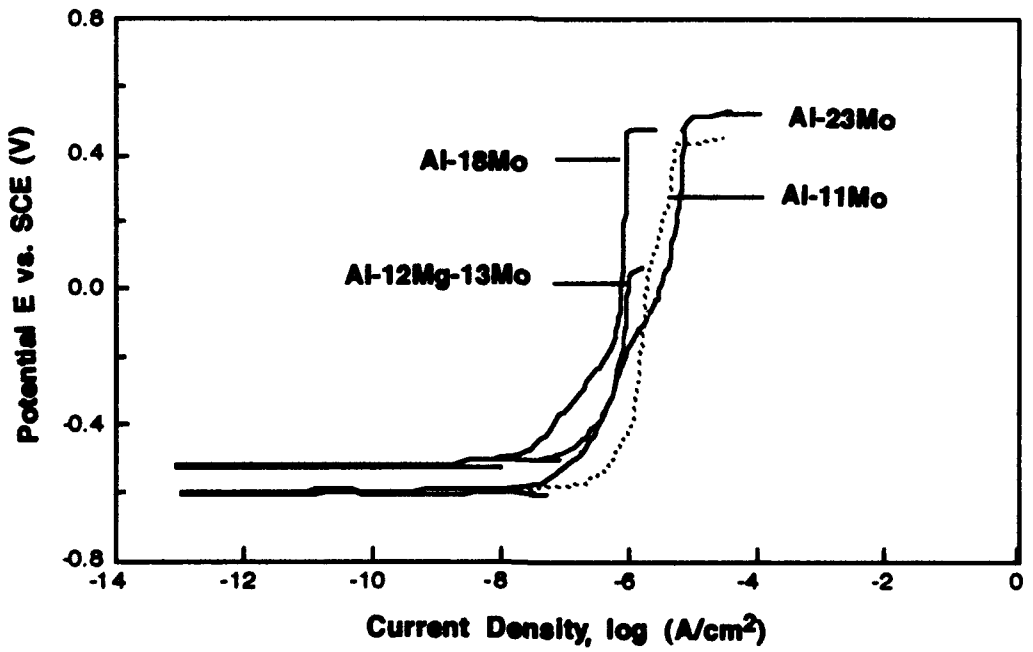

Figure 2. *Anodic Polarization Response of Various Al-Mo Alloys, Polarized in Quiescent 0.1 M NaCl, pH 8, 25°C.*

evident. Variations in i_{pass} were attributed to defects, i.e., scratches, pinholes, small cracks, etc., in the alloy film. Many of these defects are believed to result from dust particles on the surface of the Si wafer prior to deposition. Defects are also introduced when the coated Si wafers are cleaved. Some examples of these imperfections are shown in Figures 3 and 4.

Additional polarization experiments were conducted on the Al-18Mo alloy in aerated and quiescent (i.e., not aerated or deaerated) NaCl solutions (pH 8) with Cl^- concentrations of 0.1 and 0.55 M. Figure 5 shows that the anodic polarization response was not significantly altered by either increasing the Cl^- concentration, by solution aeration, or both.

Polarization response was measured for the Al-11Mo, Al-18Mo and Al-12Mg-13Mo after heat treatment at 400, 500, and 600°C for 1, 2, and 8 hrs. Although the breakdown potential for the heat treated Al-11Mo alloys (Figure 6) became more active, ~420 mV_{SCE} (as-sputtered) to 50 mV_{SCE} (heat treated), E_{corr} remained relatively constant at approximately -550 mV_{SCE}. Reduction in E_b for the Al-11Mo alloy could have resulted from the formation of precipitates during heat treatment which created microgalvanic cells with the surrounding alloy. Conversely, i_{pass} decreased from ~1 $\mu A/cm^2$ for the as-deposited alloy to ~0.1 $\mu A/cm^2$ after heat treatment. The lower i_{pass} values are likely due to the formation of a more stable or thicker oxide during heat treatment.

The Al-18Mo alloys also retained their good corrosion resistance following heat-treatment. Both E_{corr} and E_b for the Al-18Mo alloy were not dramatically affected by heat treating up to 500°C for 2 hrs (Figure 7). Passive current density values for the heat-treated Al-18Mo alloys were also similar to the as-sputtered alloy, having i_{pass} values from 0.1 to 0.5 $\mu A/cm^2$.

The Al-12Mg-13Mo alloy exhibited an E_{corr} value of -580 mV_{SCE} and E_b of 55 mV_{SCE} in the as-sputtered condition which is similar to the Al-Mo alloys (Figure 8). E_{corr} was maintained after heat treating at 400°C for 1 hr, however, heat treating the ternary alloy at longer times and higher temperatures resulted in a more active E_{corr} (approximately -800 mV_{SCE}) with no passive response during polarization.

Galvanic diagrams were generated by superimposing the anodic curve of the pure Al, 6061 Al, and Al-Mo with the cathodic curve of the P75 Gr fibers (Figure 9). This diagram reveals that the galvanic corrosion of pure sputtered and 6061 Al coupled to P75 Gr fibers is cathodically controlled with estimated coupled current densities of 12.5 $\mu A/cm^2$. For a cathodically controlled reaction, the cathodic curve shifts to a higher current density as the Gr-to-Al area ratio increases, accelerating the corrosion rate of the Al matrix (which is proportional to the cross-over point for the two curves). Converse to behavior for pure Al and 6061 Al, galvanic corrosion was anodically controlled for the Al-Mo alloys with an estimated galvanic current density of 1 $\mu A/cm^2$. For anodic controlled corrosion, changing the Gr-to-Al ratio and subsequently shifting the cathodic curve to higher current density values (or anodic curve to lower current density) would not significantly change the corrosion rate for the Al-Mo alloys. This

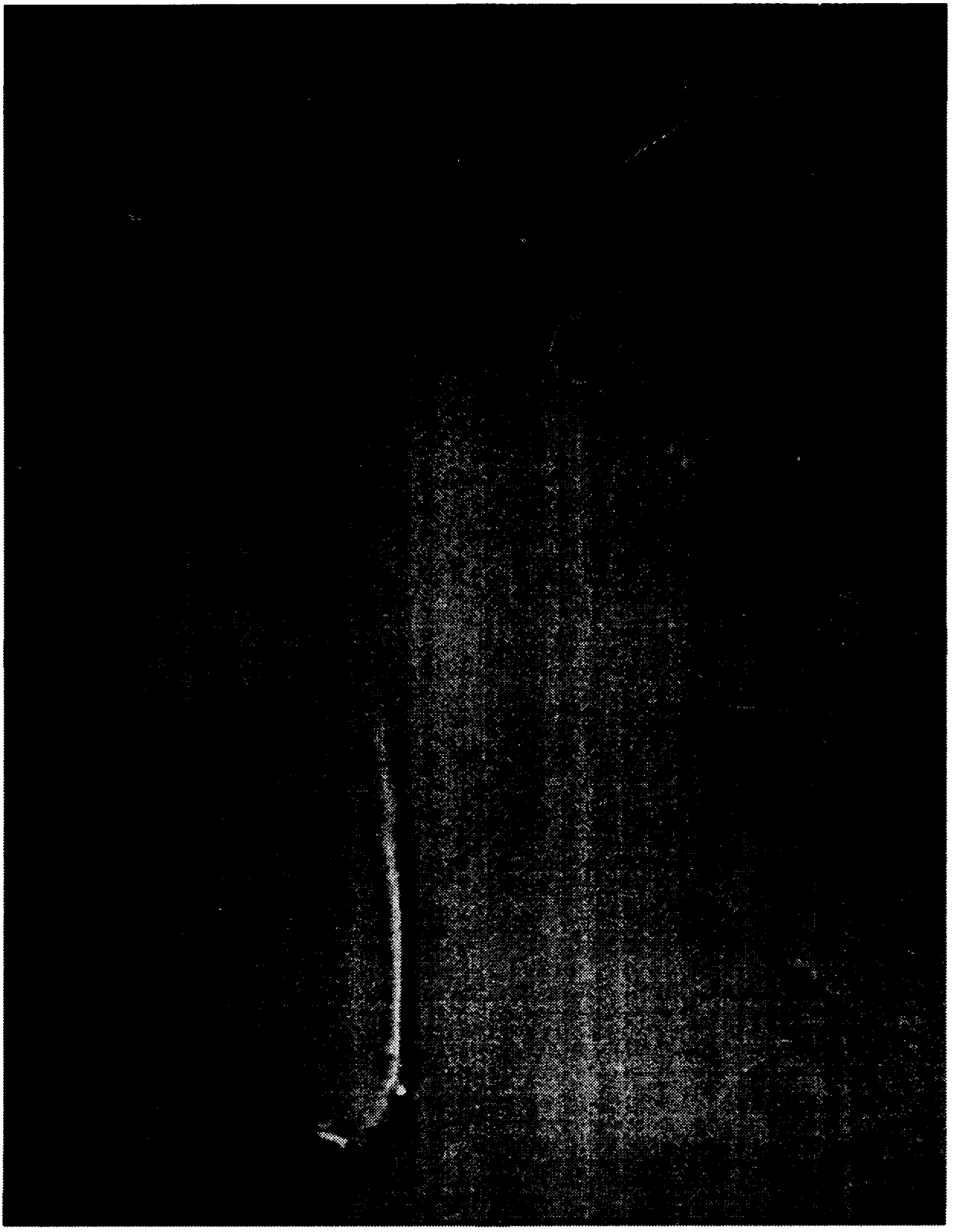

Figure 3. ***Inherent Defect on an Uncleaved, Untested Al-23W Thin Film Alloy.***

Figure 4. *Inherent Defect on an Uncleaved, Untested Al-15Mo Thin Film Alloy.*

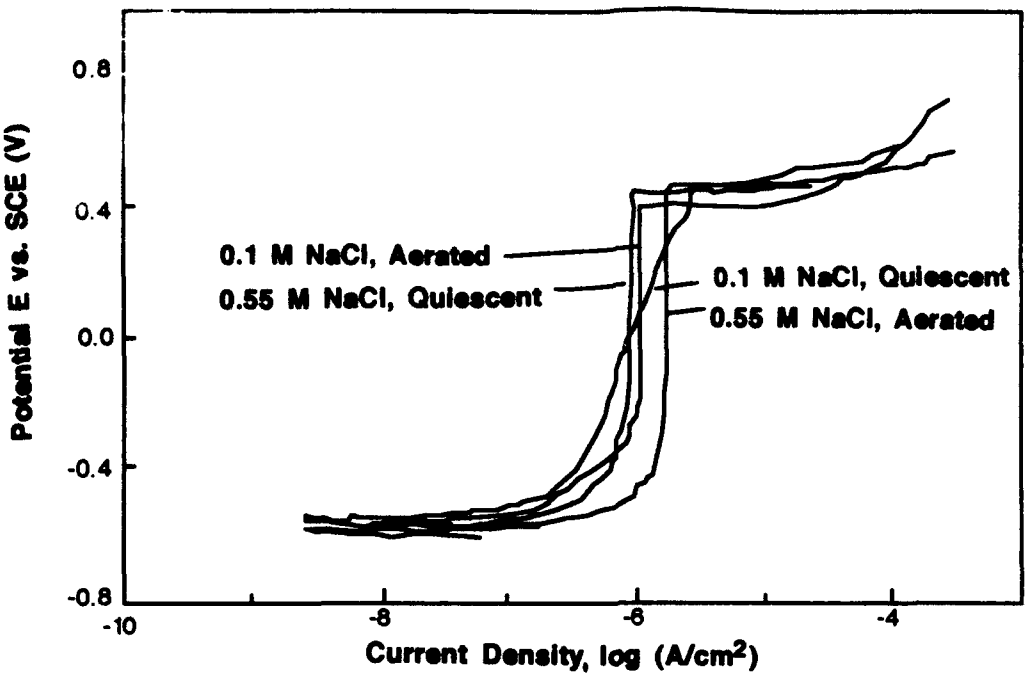

Figure 5. ***Anodic Polarization Response of Al-18 Mo Used for Detailed Heat Treatment Studies, Polarized in Quiescent and Aerated 0.1M and 0.55M (3.15 wt. %) NaCl, pH 8, 25°C.***

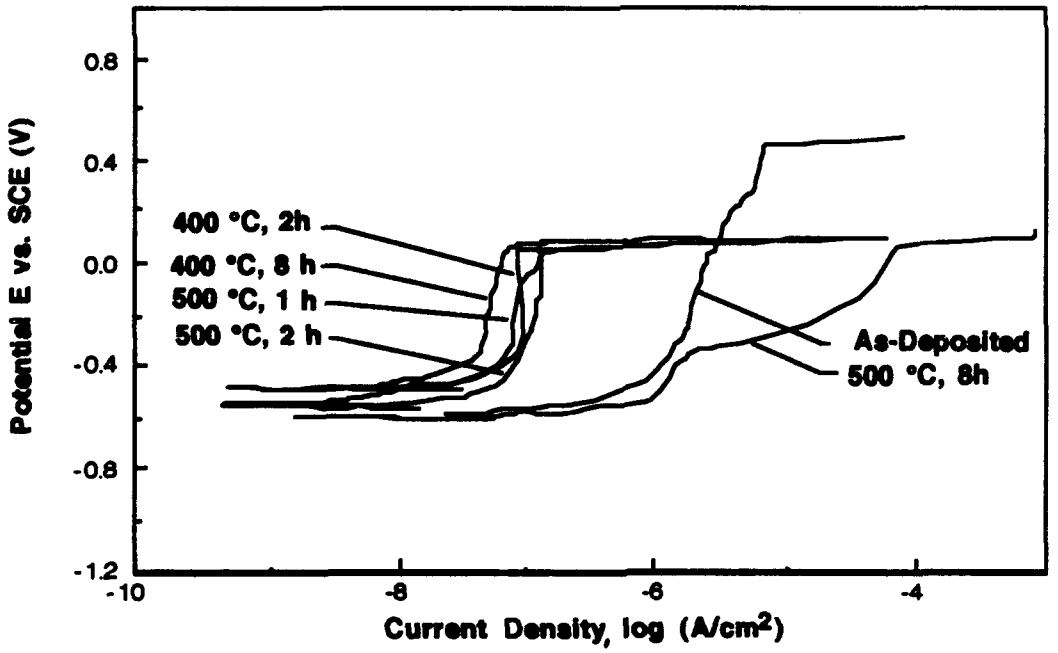

Figure 6. ***Anodic Polarization Response of Al-11Mo Alloy Before and After Heat Treatment at 400°C for 1 and 2 h and 500°C for 1, 2, and 8 h, Polarized in Quiescent 0.1 M NaCl, pH 8, 25°C.***

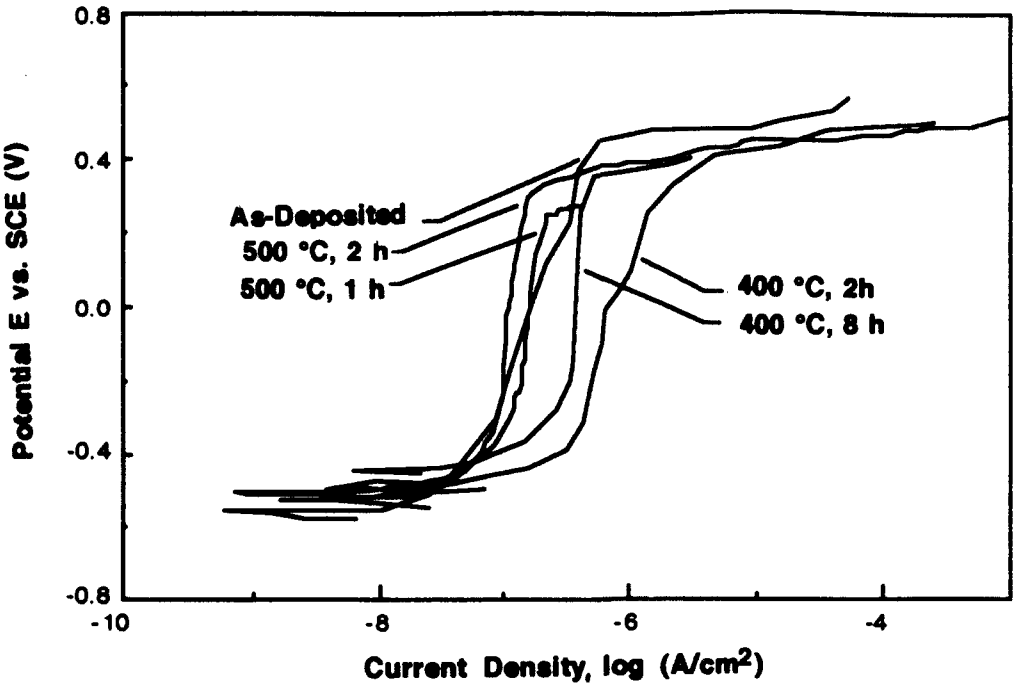

Figure 7. ***Anodic Polarization Response of Al-18Mo Alloy Before and After Heat Treatment at 400°C for 2 and 8 h and 500°C for 1 and 2 h, Polarized in Quiescent 0.1 M NaCl, pH 8, 25°C.***

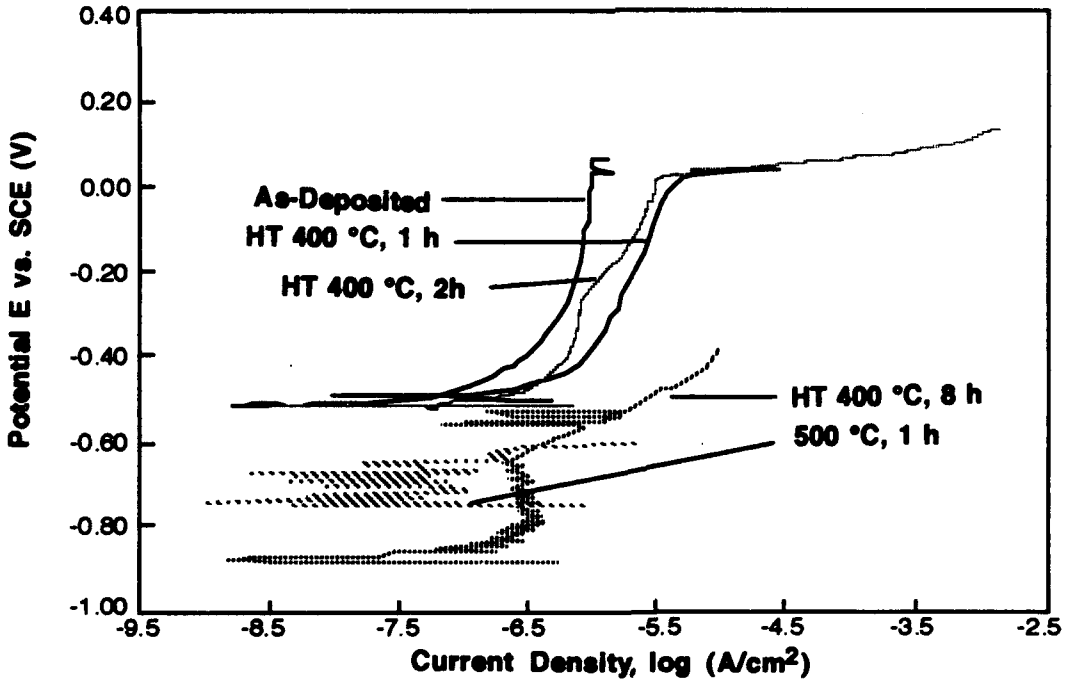

Figure 8. ***Anodic Polarization Response of Al-12Mg-13Mo Before and After Heat Treatment at 400°C for 1, 2 and 8 hrs and 500°C for 1 hr, Polarized in Quiescent 0.1M NaCl, pH 8, 25°C.***

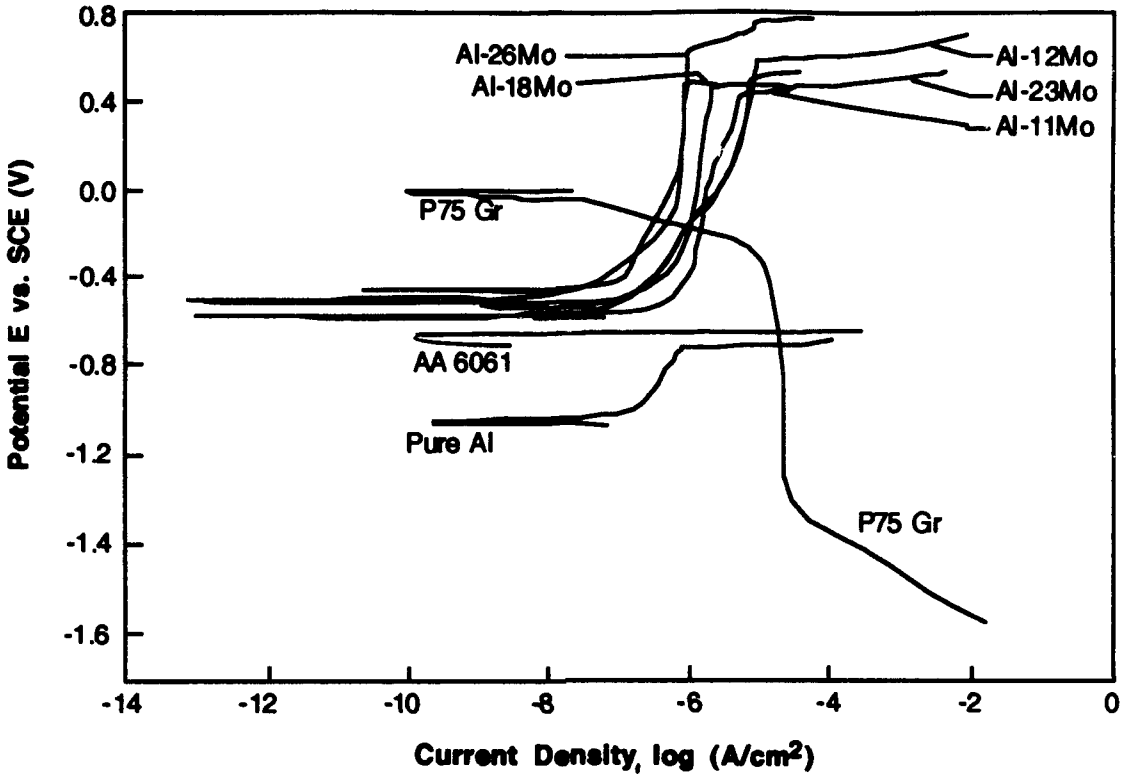

Figure 9. ***Galvanic Diagram with Anodic Curve of Pure Sputtered Aluminum, Wrought 6061 Al, and Various Sputtered Al-Mo Alloys Combined with the Cathodic Curve for an Equal Area of P75 Graphite Fibers, Tested in Quiescent, 0.1M NaCl, pH 8, 25°C.***

result is important because modifying the Gr fiber volume, which is a key design feature of composites to achieve specific thermal or mechanical properties, will not result in dramatic changes in the corrosion response of the Gr/Al-Mo composite.

The galvanic corrosion reaction remained anodically controlled for both the Al-11Mo (Figure 10) and Al-18Mo (Figure 11) alloys after heat treatment. Although some of the Al-11Mo and Al-18Mo alloys precipitated during heat treatment, they still exhibited passive polarization response and the galvanic diagrams predict the corrosion will be controlled by the anodic dissolution of metal. Only after heat treating the Al-11Mo to 500°C for 8 hrs was control for the galvanic reaction changed from anodic (Al passivation) to cathodic (oxygen reduction on Gr fibers).

To confirm the predictions made using the galvanic diagrams, long term galvanic current tests were conducted on sputtered Al, Al-11Mo, Al-18Mo, Al-23Mo, and ternary Al-12Mg-13Mo in the as-deposited condition by coupling the alloy to P75 Gr fibers (Figure 12). Galvanic current values are equivalent to galvanic current densities (i_{galv}) since the anode areas were 1 cm^2. For all the alloys, the galvanic current initially starts off at relatively high values between 3 and 30 $\mu A/cm^2$, but quickly drops to a low steady state value. The Al-18Mo and Al-23Mo reached low measured galvanic current densities of ~0.04 and ~0.08 $\mu A/cm^2$, respectively which were up to three orders of magnitude lower than the galvanic current density values of 30 $\mu A/cm^2$ measured for pure sputtered Al. Current densities of the Al-18Mo alloys after heat treatment at 400°C for 2 hrs were comparable to the as-sputtered value of 0.08 $\mu A/cm^2$. Even after heat treatment at 500°C for 2 hrs, the galvanic current density was an order of magnitude lower than that of pure sputtered Al. After galvanic testing for seven days (605 ks) the pure sputtered Al had completely dissolved from the Si wafer whereas the Al-Mo alloys remained intact and highly specular. The Al-12Mg-13Mo alloy exhibited a galvanic current value of 10 $\mu A/cm^2$ which is greater than the binary Al-Mo alloys but still 3 times lower than for pure Al. However, in less than 12 hrs (40 ks) following immersion in the 0.1 M NaCl, pH 8, solution, the Al-Mg-Mo alloys coupled to P75 Gr fibers had exfoliated and completely lifted away from the sapphire wafer. Due to the short time in solution for the Al-12Mg-13Mo alloy, data for this alloys is not included in Figure 12.

XRD results for the Al-Mo alloys heat treated at 400, 500, and 600°C for 1, 2, and 8 hr are summarized in Table 1. XRD patterns revealed that the as-sputtered alloys were amorphous as evident by a large broad peak centered at 41° shown in the representative XRD pattern in Figure 13. After heat treatment some alloys formed precipitates but many of the alloys remained amorphous. Table 1 shows that as the concentration of Mo increases, the propensity for the alloy to precipitate decreased. For example, the Al-11Mo formed precipitates at the lowest time and temperature (1 hr, 400°C), whereas the Al-23Mo alloy did not form precipitates until after heat treatment at 600°C for 8 hrs. Lack of precipitates in the alloys with higher Mo concentrations suggests the atomic mobility significantly decreases. Reduction in atomic mobility could be

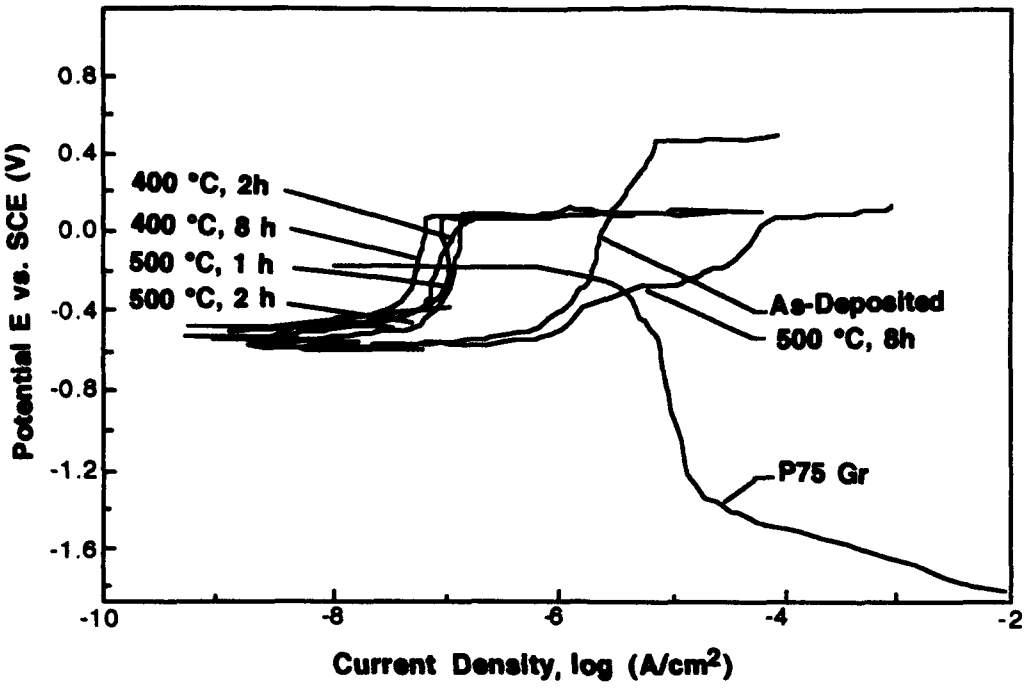

Figure 10. ***Galvanic Diagram for Equal Areas Al-11Mo Alloy Before and After Heat Treatment at 400° for 2 and 8 h and 500°C for 1, 2, and 8 h With P75 Gr Fibers, Tested in Quiescent 0.1 M NaCl, pH 8, 25°C.***

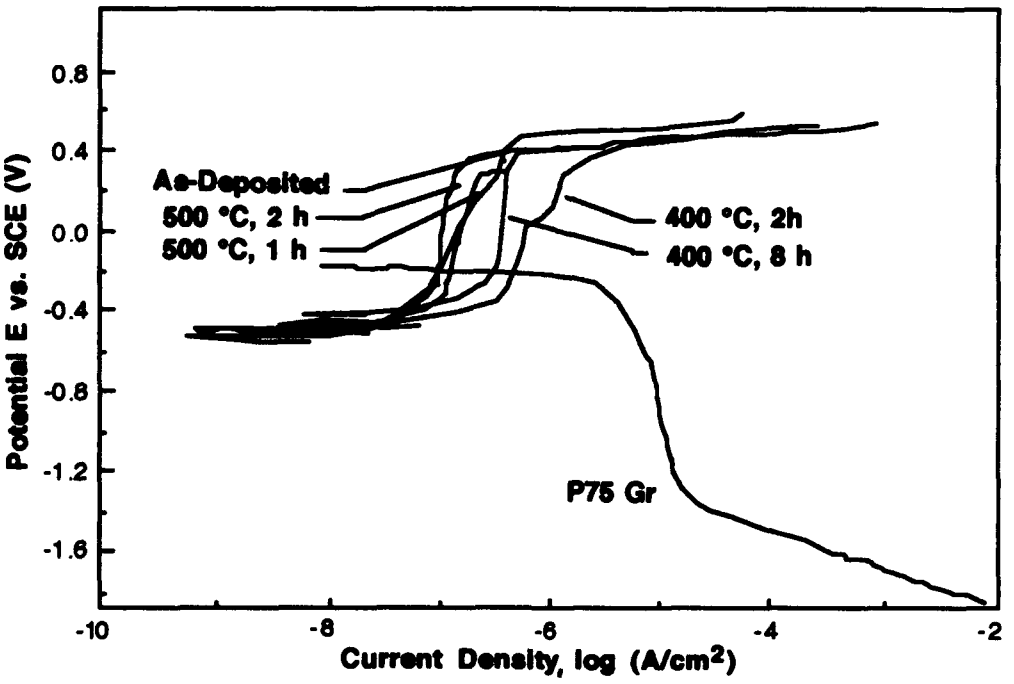

Figure 11. ***Galvanic Diagram for Equal Areas Al-18Mo Alloy Before and After Heat Treatment at 400°C for 2 and 8 h and 500°C for 1 and 2 h With P75 Gr Fibers, Tested in Quiescent 0.1 M NaCl, pH 8, 25°C.***

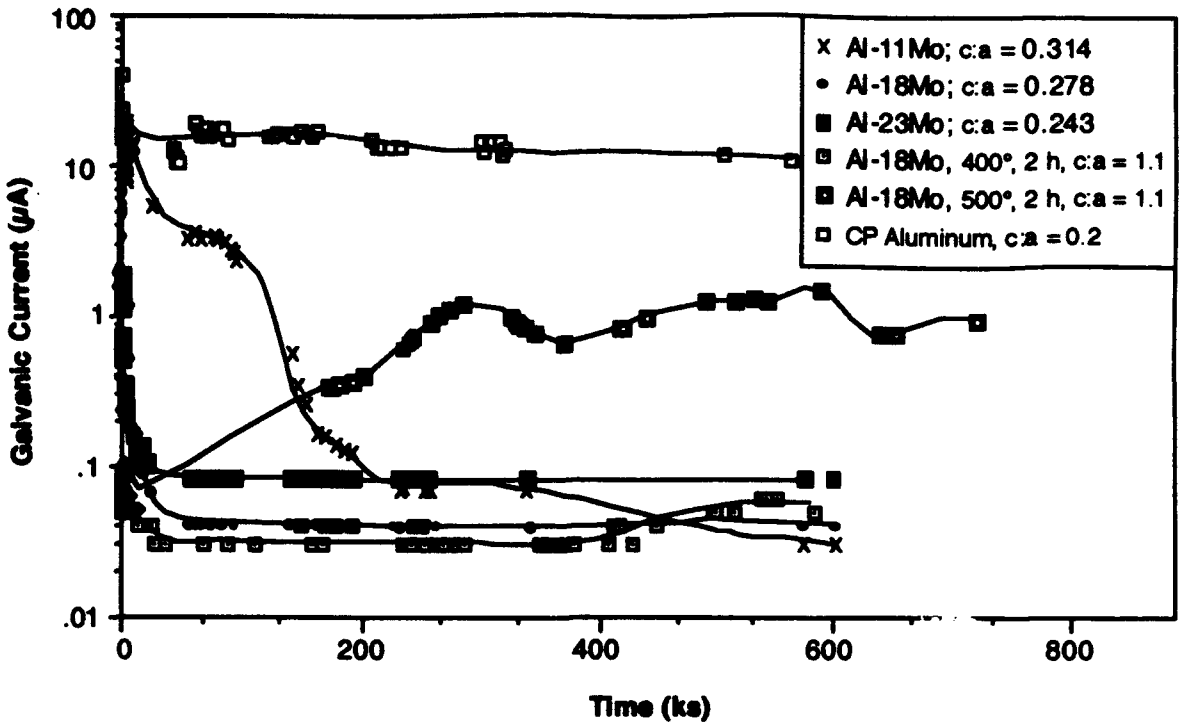

Figure 12. ***Galvanic Current for Commercially Pure Aluminum and Al-18Mo Alloys (As-Deposited and Heat Treated) Coupled to P75 Graphite Fibers in Quiescent 0.1M NaCl, pH 8, 25°C.***

Table 1. ***Summary of Al-Mo Alloy Structure as a Function of Heat Treatment Time and Temperature.***

Heat Treatment Time (hrs)	Heat Treatment Temperature		
	400°C	500°C	600°C
1	Al-11Mo, ppt Al-18Mo, Amorphous Al-23Mo, Amorphous	Al-11Mo, ppt Al-18Mo, ppt Al-23Mo, Amorphous	Al-11Mo, ppt Al-18Mo, ppt Al-23Mo, Amorphous
2	Al-11Mo, ppt Al-18Mo, Amorphous Al-23Mo, Amorphous	Al-11Mo, ppt Al-18Mo, ppt Al-23Mo, Amorphous	Al-11Mo, ppt Al-18Mo, ppt Al-23Mo, Amorphous
8	Al-11Mo, ppt Al-18Mo, Amorphous Al-23Mo, Amorphous	Al-11Mo, ppt Al-18Mo, ppt Al-23Mo, Amorphous	Al-11Mo, ppt Al-18Mo, ppt Al-23Mo, ppt

ppt - fully precipitated

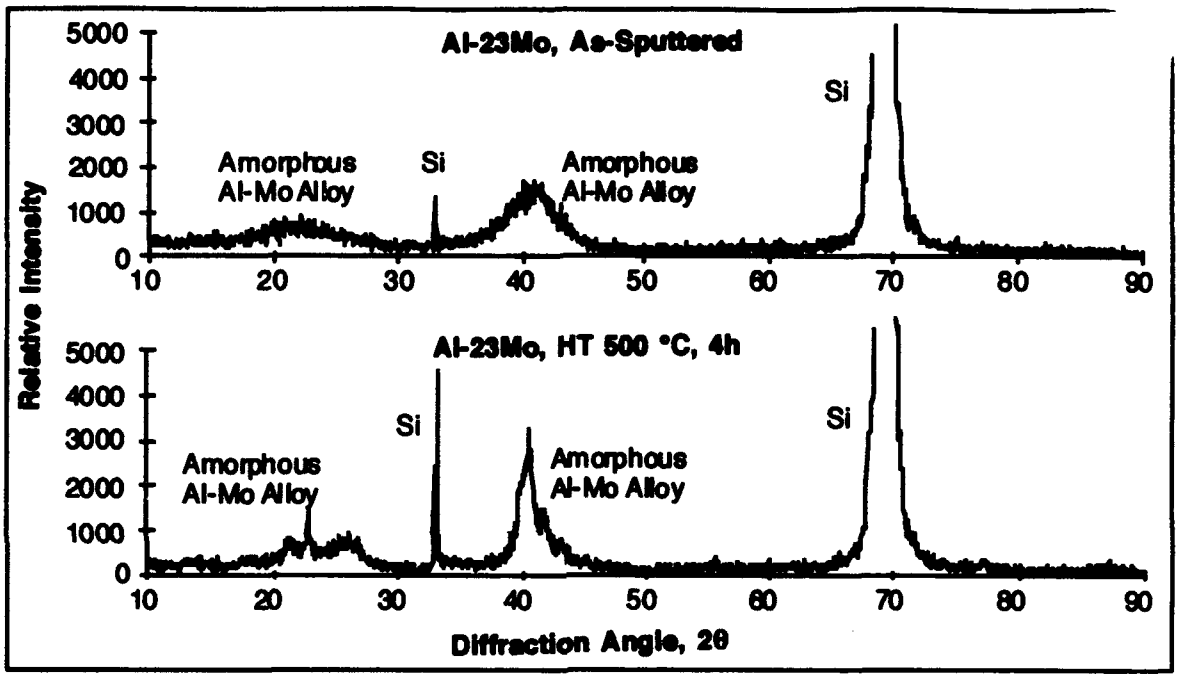

Figure 13. ***X-ray Diffraction of Al-23Mo Alloy in the As-Sputtered Condition and After Heat Treatment. As-Sputtered, the Alloy is Amorphous and it is Just Beginning to Precipitate After Heat Treatment at 500°C for 2 h.***

attributed to a more random structure or due to second neighbor interaction (i.e., Mo-Mo atom interaction).

Transmission electron microscopy was conducted on the Al-18Mo in the as-sputtered condition and after heat treatment at 400°C for 2 and 8 hrs and 500°C for 2 and 8 hours. Figure 14 shows the representative structure of the as-sputtered alloy with the corresponding selected area diffraction (SAD) pattern. Structure of the as-deposited Al-Mo alloy is featureless with the exception of the mottled appearance that resulted from the extensive ion milling used to thin the specimen. The SAD pattern shows two diffuse rings that correspond to the d-spacing calculated for the broad peaks found on the XRD patterns. Similar structures and SAD patterns were obtained for the Al-18Mo alloy heat treated at 400°C for 2 and 8 hr which correlates with the XRD patterns that showed that the alloy remained amorphous after heat treatment. After heat treatment to 500°C for 2 and 8 hr small precipitates began to appear (Figure 15). SAD of these precipitates indicate a structure of $Al_{12}Mo$, Al_5Mo, and Al. As with XRD not all the rings for each phase could be indexed and many of the rings could not be correlated with the expected Al-Mo intermetallic compounds. SAD of the Al-18Mo alloy heat treated at 500°C for 8 hr shows an elongation of the diffraction spots which arises from fine precipitates that are preferentially oriented.

Al-Ti

Polarization and long-term galvanic tests of several sputter deposited non-equilibrium Al-Ti and Al-Mg-Ti alloys were also performed this year. Anodic polarization was performed on Al-50Ti, Al-5Mg-19Ti, and Al-10Mg-14Ti at scan rates of 0.2 and 0.05 mV/s in 0.1 M NaCl at adjusted pH values of 3, 8, and 12. Long-term galvanic testing was performed by coupling graphite to the alloys through a zero resistance ammeter and measuring the current between the two materials.

Figures 16 through 18 show anodic polarization behavior for different Al-Ti alloys tested in pH 3, 8, and 12 chloride solution, respectively. Significant improvements in corrosion resistance are observed for these alloys when compared to pure Al at all pH values tested. E_b values for the alloys tested in pH 3 Cl^- solution ranged from -300 mV_{SCE} to +300 mV_{SCE} while tests conducted at pH 8 and 12 resulted in E_b values greater than 0 mV_{SCE}. Passive current densities for these alloys were generally low, with the largest value being 38 $\mu A/cm^2$ for Al-10Mg-14Ti tested in pH 3 chloride solution.

Several trends were noted when increasing the pH between 3 and 12. First, E_{corr} consistantly decreased when increasing the solution pH for all three alloys. For example, E_{corr} for Al-5Mg-19Ti was approximately -630 mV_{SCE} at pH 3, decreasing to -880 mV_{SCE} at pH 8, and finally decreasing to -1130 mV_{SCE} at pH 12. Second, E_b values tended to become more noble with increasing solution pH. Al-58Ti exhibited an E_b value of +300 mV_{SCE} at pH 3 to greater than +2000 mV at a pH value of 12. No trend was noted for i_{pass} with increasing pH.

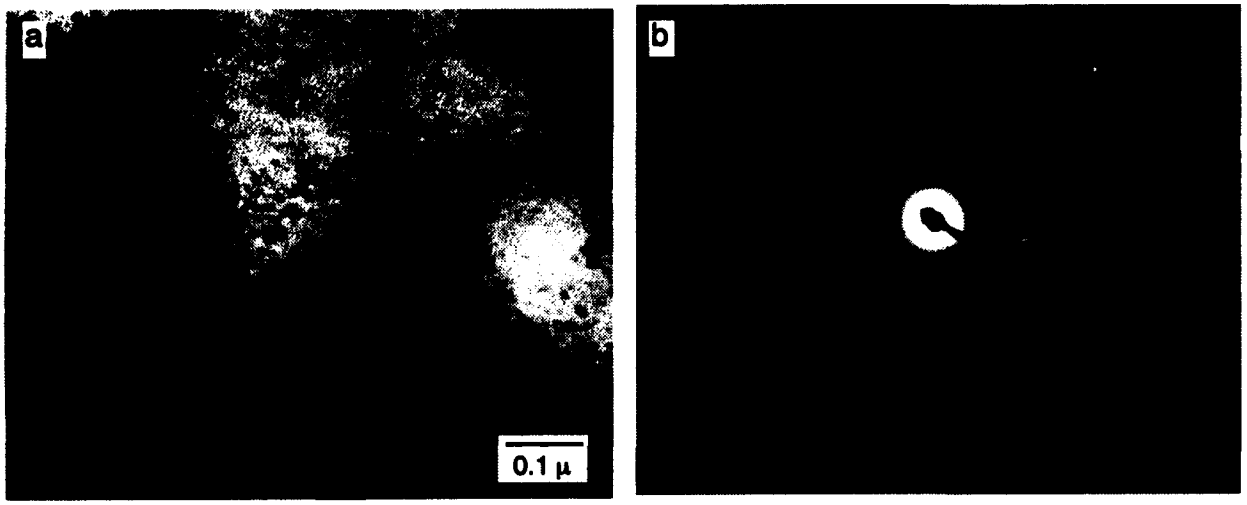

Figure 14. ***Representative Structure (a) and Associated Selected Area Diffraction Pattern (b) for Amorphous Al-18Mo in the As-deposited Condition and After Heat Treatment at 400°C for 2 and 8 h.***

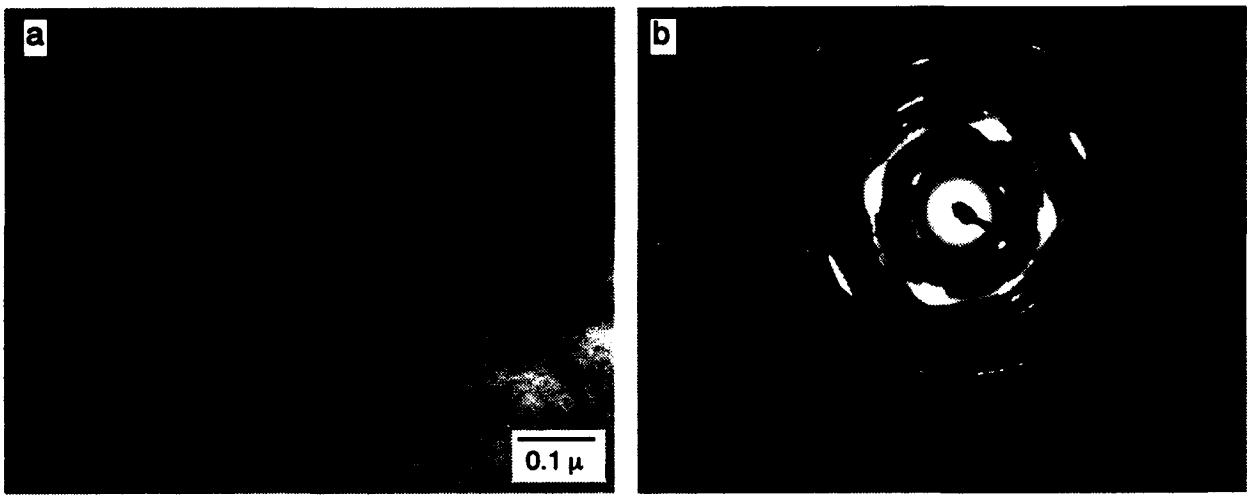

Figure 15. ***Structure (a) and Selected Area Diffraction pattern (b) for the Al-18Mo Heat Treated at 500°C for 8 h. Fine Elongated Precipitates are Evident and the SAD Pattern Shows Elongated Spots that Correspond to the Fine Precipitate Structure.***

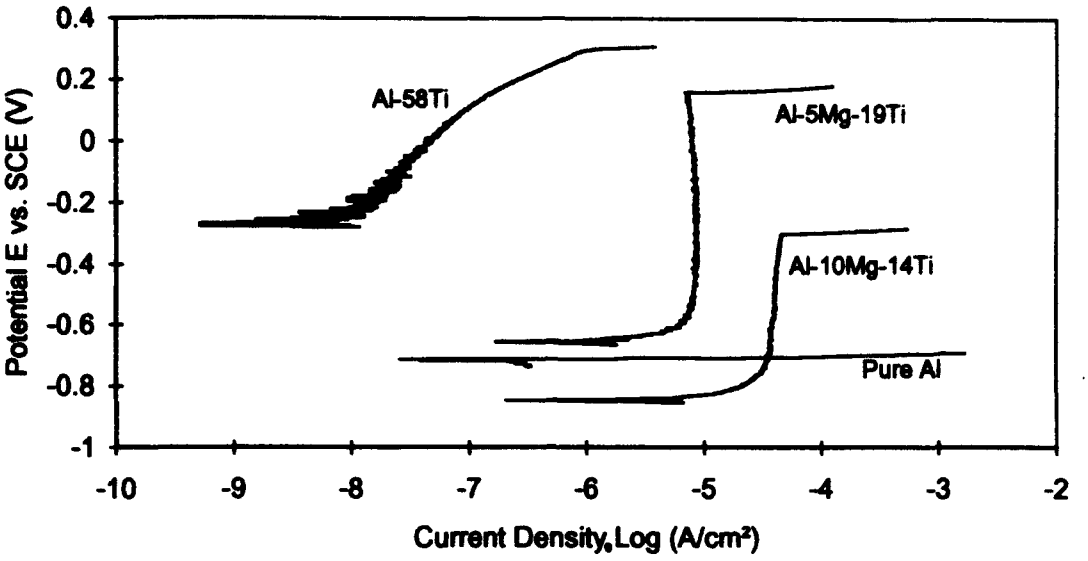

Figure 16. Potentiodynamic Scans of Al-58Ti, Al-5Mg-19Ti, Al-10Mg-14Ti, and Pure Al in 0.1 M NaCl at pH 3 at a Scan Rate of 0.2 mV/s.

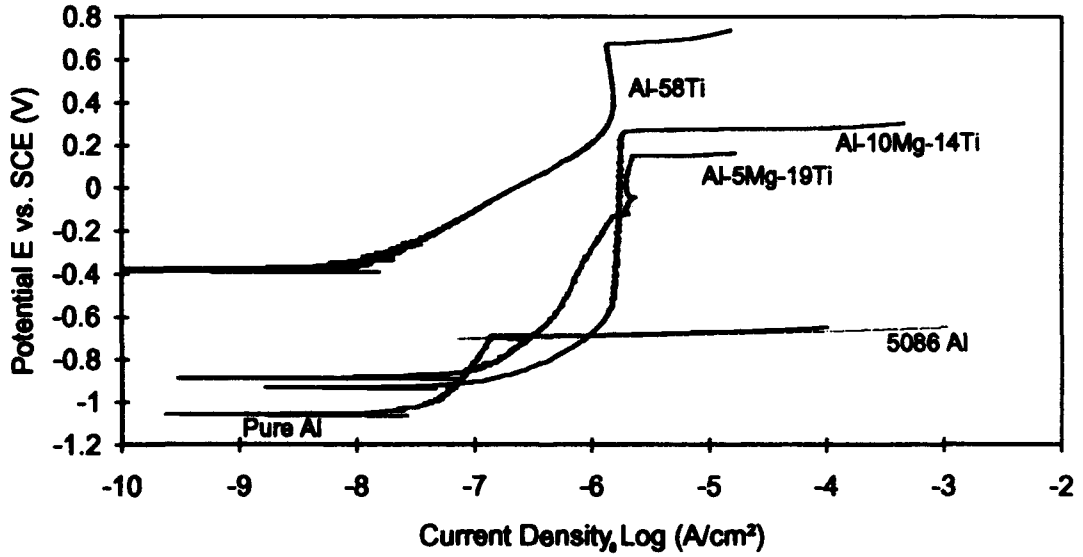

Figure 17. Potentiodynamic Scans of Al-58Ti, Al-5Mg-19Ti, Al-10Mg-14Ti, Pure Al, and 5086 Al in 0.1 M NaCl at pH 8 at a Scan Rate of 0.2 mV/s.

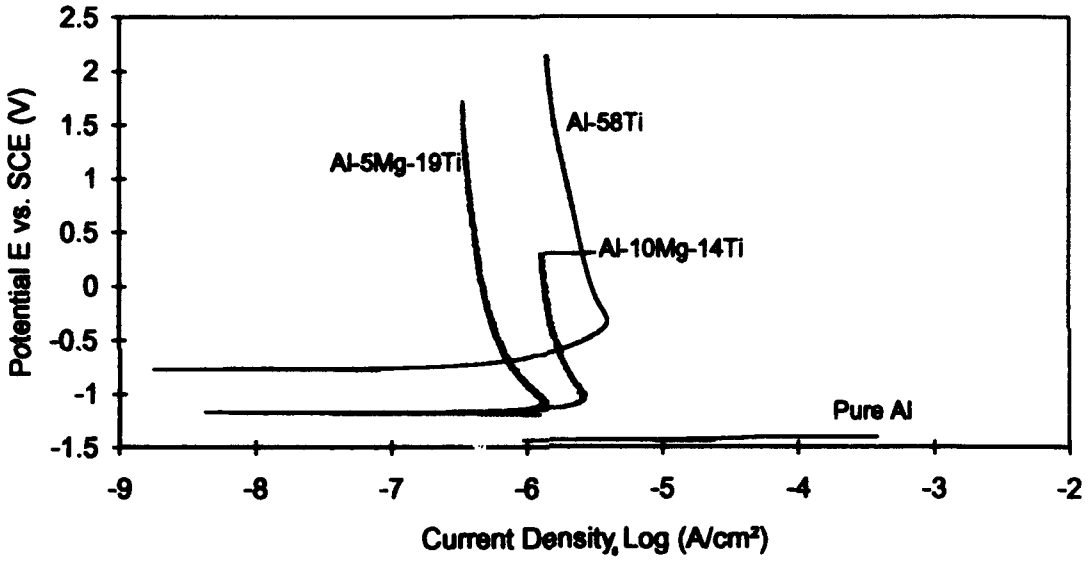

Figure 18. Potentiodynamic Scans of Al-58Ti, Al-5Mg-19Ti, and Al-10Mg-14Ti in 0.1 M NaCl at pH 12 at a Scan Rate of 0.05 mV/s and Pure Al at 0.2 mV/s.

Since these alloys may be considered for use in MMCs, galvanic corrosion between the graphite reinforcing fibers and the alloy matrix is an important concern. In order to evaluate this, two previously described methods, galvanic diagrams and long-term galvanic testing, were employed for assessing galvanic compatibility. Figure 19 shows galvanic diagrams for several alloys tested in pH 8 solution. Table 2 summarizes the results obtained from overlaying the alloy anodic and graphite cathodic polarization curves. Pure Al was under cathodic control at all pH values. The Al-10Mg-14Ti was also cathodically controlled at the pH value of 3. Again, when the galvanic couple is under cathodic control, a small change in cathode (i.e., graphite) area results in a significant change in the coupled current density. In all of the other overlays anodic control was maintained, indicating that a change in graphite area would not significantly alter i_{galv}.The second method used for evaluating galvanic corrosion is long-term coupling of the Al-Ti and Al-Mg-Ti alloys with graphite. Figure 20 shows a plot of current versus time for three of these alloys. The cathode-to-anode ratios were selected based upon two criteria. First, the approximate ratio of the metal matrix to reinforcing fibers (simulating an approximate 65 % matrix - 35 % fiber) was used, and second, a small amount of exposed graphite in the presence of a large alloy matrix was simulated by having a very small graphite area (approximately 0.02 cm^2). Both Al-58Ti and Al-10Mg-14Ti exhibited extremely low currents (< 0.02 μA, corresponding to 0.02 $\mu A/cm^2$ for Al-10Mg-14Ti and 0.007 $\mu A/cm^2$ for Al-58Ti) while the Al-5Mg-19Ti had a slightly higher current of approximately 0.1 μA (0.07 $\mu A/cm^2$).

Graphite Fiber Coating

Al alloyed with 11 to 18 atomic percent Mo was targeted as the optimum alloy composition for use in a MMC because these alloys retained the improved corrosion resistance after heat treatment (at 400 °C) while minimizing the impact of higher Mo concentrations on the alloy density. Several fiber coating trials were conducted on a commercial in-line sputter system, at Cordec, Inc., Lorton VA, designed for rapid deposition of alloys onto graphite fibers. Targets were fabricated by machining slots into high purity (99.99%) Al plates and inserting high purity (99.9%) Mo slugs. Composition was controlled by modifying the area ratio of Mo to Al in the target. Initially, a hollow cathode configuration was investigated, but the alloy coated fibers contained residual stresses that caused the fibers to curl. Therefore a upper and lower planar target arrangement was used to coat the graphite fibers. Details and results of both the hollow cathode and planar cathode methods are presented in the following paragraphs. Amoco P75 and P120, and DuPont E120 Gr fiber tows containing 2000-7 μm diameter fiber filaments were coated in this study. Alloy thickness on the fiber was targeted at 3 μm to achieve a consolidated composite fiber volume of 50 % as shown in Figure 21.

Initially a hollow cathode magnetron configuration was used in which the spread fibers pass through the center of a cylindrical cathode. The advantage of the hollow cathode is the thickness of the alloy is very uniform around the fiber and the target yield is high (>90%). The hollow cathode was fabricated from a pure aluminum hollow cylinder with Mo plugs. Approximately 90 g (280

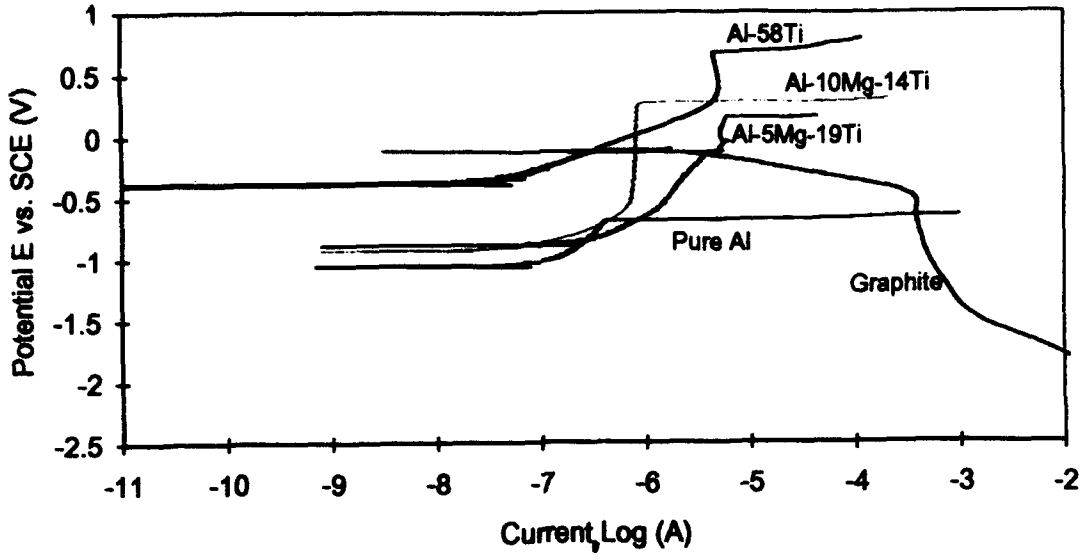

Figure 19. Galvanic Overlay of Graphite Cathodic Polarization Curve and Anodic Polarization Curves of Al-58Ti, Al-5Mg-19Ti, Al-10Mg-14Ti, and Pure Al in 0.1 M NaCl at pH 8.

Table 2. Summary of Galvanic Current Densities Obtained using Polarization Overlays.

Alloy	i_{galv} ($\mu A/cm^2$)		
	pH = 3	pH = 8	pH = 12
Al-58Ti	0.04	0.07	4.7
Al-10Mg-14Ti	95	2.1	2.0
Al-5Mg-19Ti	12	1.2	0.59
Pure Al	670	130	1200

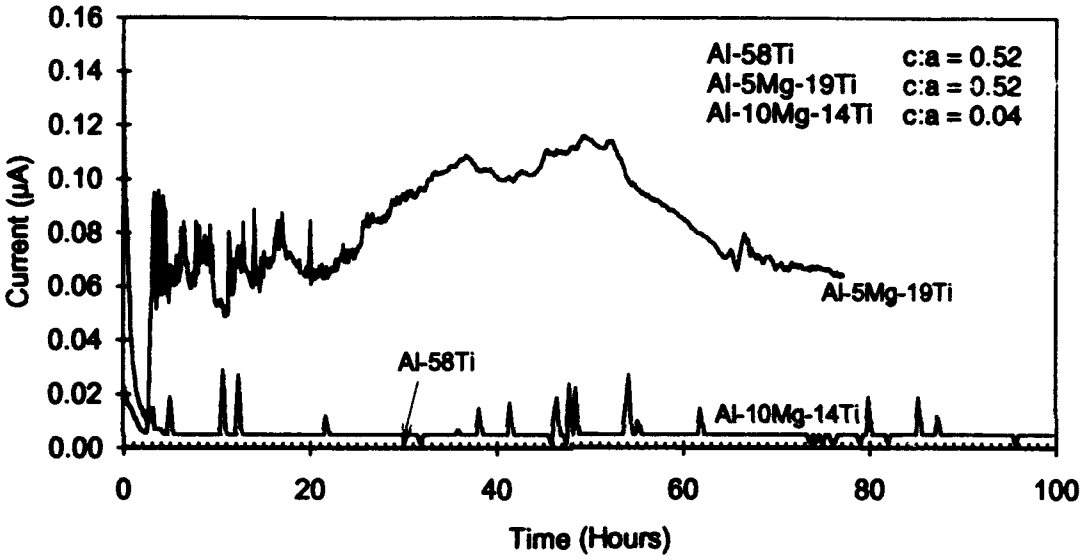

Figure 20. Galvanic Diagram of Al-58Ti, Al-5Mg-19Ti, and Al-10Mg-14Ti Coupled to Graphite in 0.1 M NaCl at pH 8.

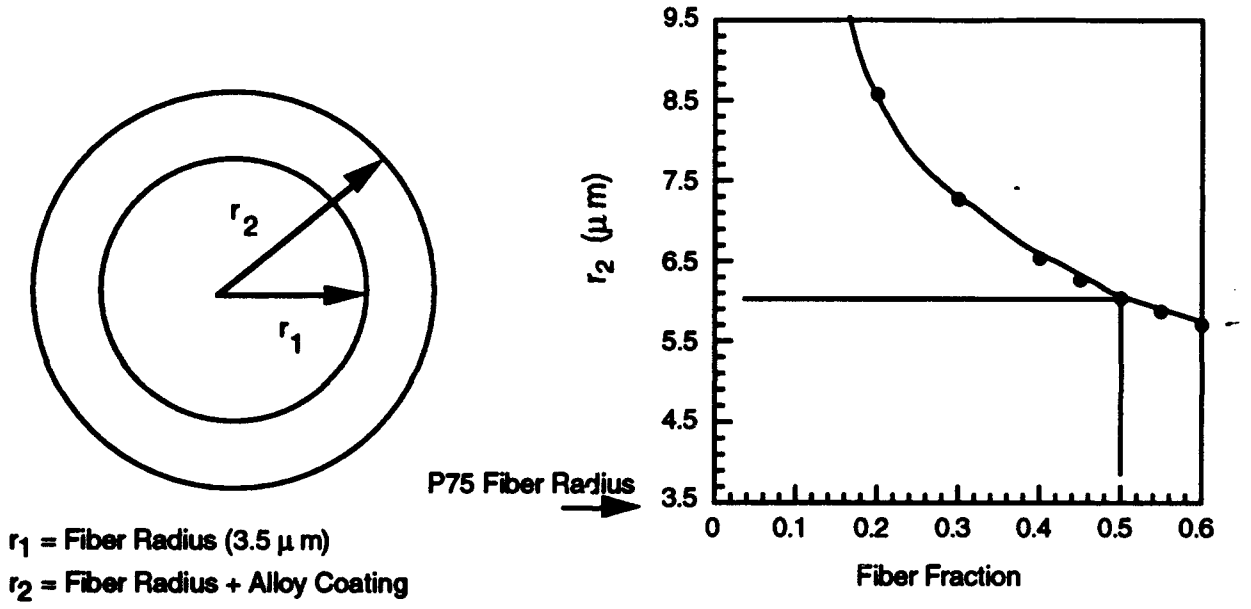

Figure 21. ***Fiber Volume of the Final Composite can be Modified by Controlling the Thickness of the Alloy Coating on the Fiber.***

meters) of fiber were coated in the hollow cathode configuration. Although the fiber coating was fairly uniform, SEM/EDS analysis indicated a Mo concentration of only 3 atomic percent. In addition, the alloy coating was in compression and caused to the fibers to curl when removed from the mandrel. The curling made it very difficult to handle the fibers and as a result the hollow cathode configuration was discontinued.

A planar cathode configuration was then considered for fiber coating. In this process, spread fibers are passed between upper and lower planar cathodes (15 x 8 in.) illustrated in Figure 22. The cathode targets were fabricated from pure Al with slots machined for Mo plugs that cross the target. Initially the Al:Mo ratio was scaled proportional to the area ratio used in the hollow cathode experiment to achieve 15 to 18 atomic percent Mo. This target configuration was used to coat approximately 100 meters of fibers. Although the coating was uniform, EDS compositional analysis indicated the Al alloy contained approximately 30 atomic percent Mo. In the next trail run half of the Mo plugs were removed and an additional ~100 meters of fibers were coated. EDS analysis of this run indicated a Mo concentration of 17 atomic percent. Once a Mo concentration of 17 atomic percent was achieved, 0.91 kg (2800 meters) of fiber were coated. Figure 23 shows the representative morphology of the Al-14Mo coated P120 graphite fiber. The ~2 to 3 μm thick coating is relatively uniform and exhibits a morphology similar to the conventional pure Al and 6061 Al alloy coated Gr fibers.

X-ray diffraction of the alloy coated fibers (Figure 24) revealed that the alloy contains both some amorphous material as indicated by the broad peak at diffraction angles of 21° and 41° (similar to alloys that were sputtered onto Si wafers) and some crystalline material which was indexed to aluminum shifted to slightly higher diffraction angles. From the diffraction angles, d values were calculated for each peak using Bragg's law.[11] Using the space lattice relationship for a cubic structure:

$$\frac{1}{d^2} = \frac{h^2 + k^2 + l^2}{a^2}$$

a lattice parameter, a, of 4.010 Å was calculated for the crystalline Al-Mo. Since Mo is in solid solution in Al, the atomic percent of Mo can be calculated based on peak shift according to Figure 25. The lattice parameter, a, for a face center cubic structure can be calculated using simple geometry and the radius of the atoms:

$$a^2 + a^2 = (2r)^2$$

$$a = 2\sqrt{2}\, r$$

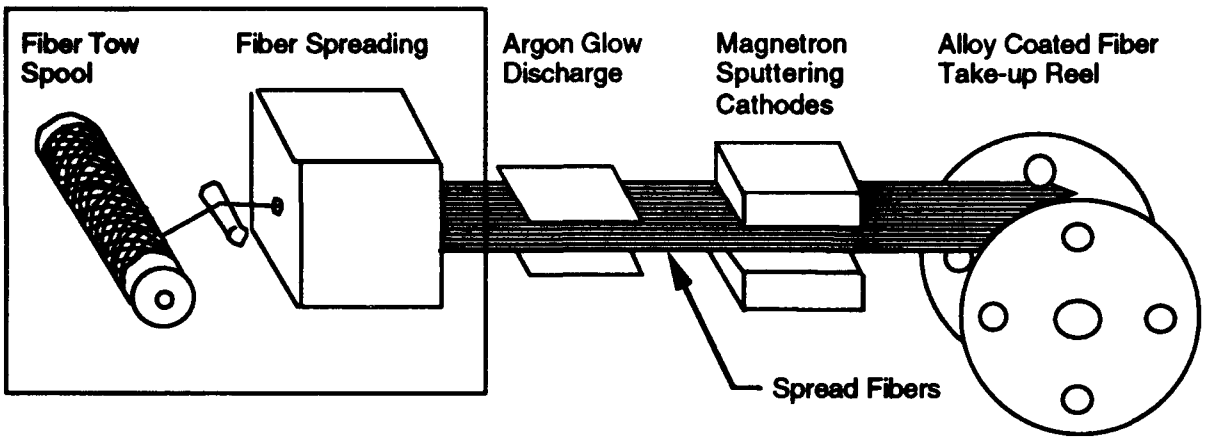

Figure 22. ***Schematic of the Physical Vapor Deposition Process using the Upper and Lower Planar Magnetron Cathodes.***

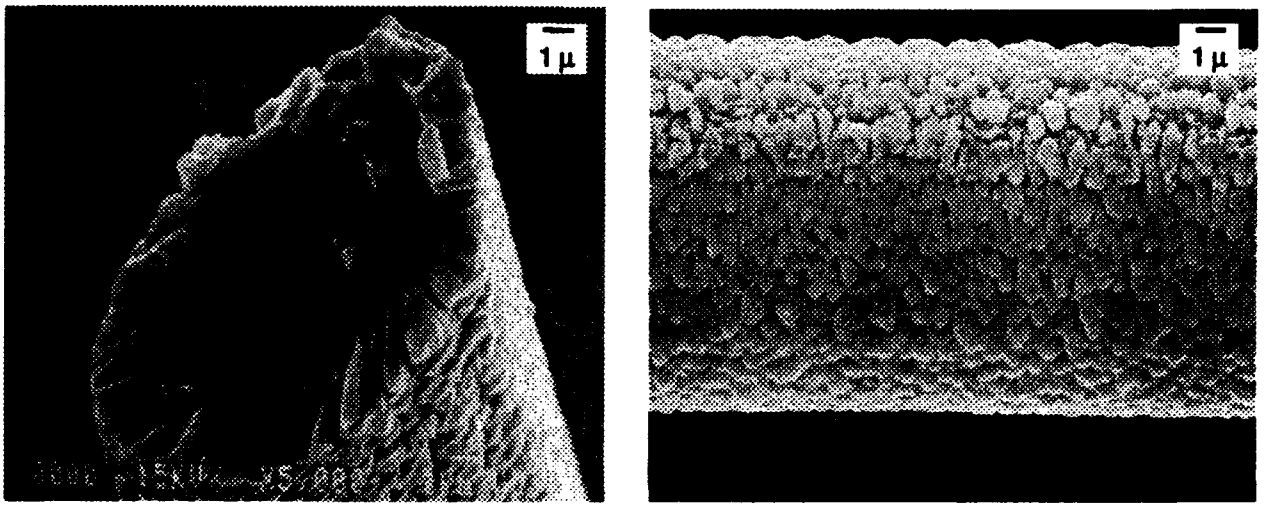

Figure 23. ***SEM micrographs of the Al-17Mo Alloy Coated P120 Gr fibers. These Micrographs Show a Uniform Coating Thickness that has Grown Radially Outward from the Fibers.***

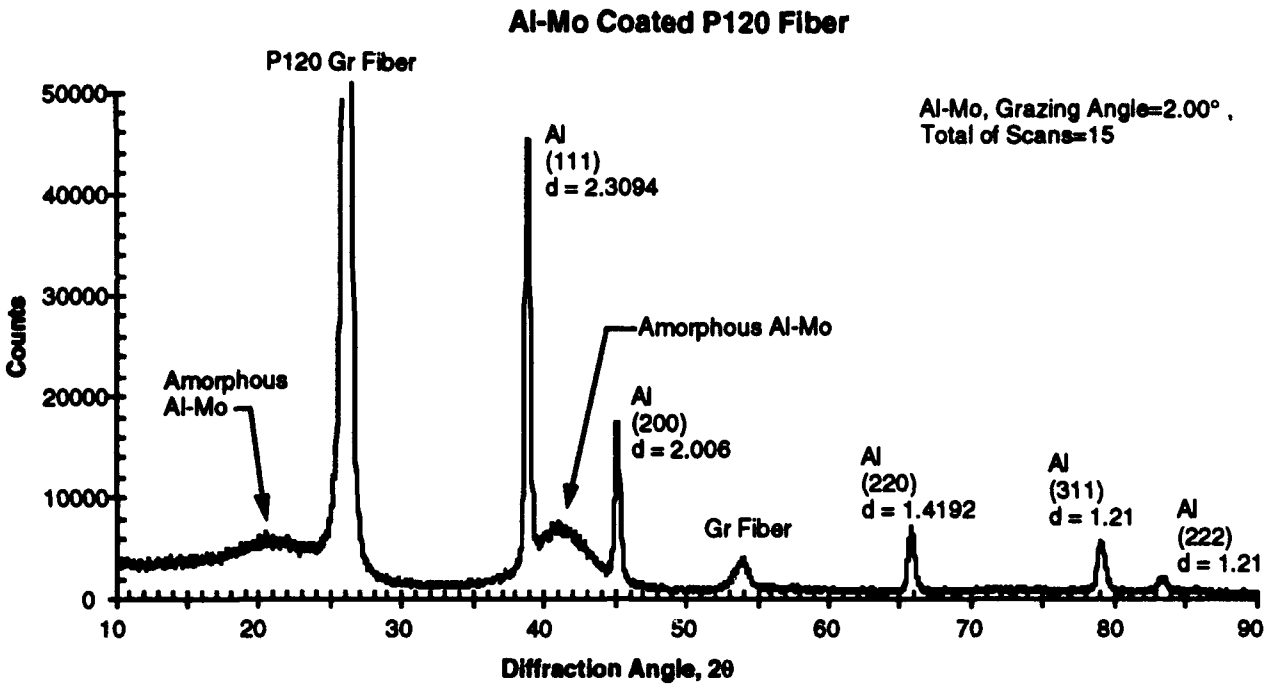

Figure 24. ***X-ray Diffraction Pattern of the Al-17Mo Alloy Coated P120 Gr Fiber Showing the Presence of both an Amorphous Phase and a Solid Solution Phase of Mo in FCC Al.***

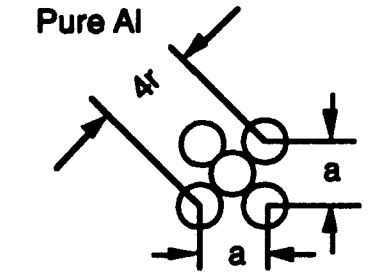

$$a^2 + a^2 = (4r)^2$$

$$a = r \cdot 2\sqrt{2}$$

a = Lattice Parameter
r = Atom Radius

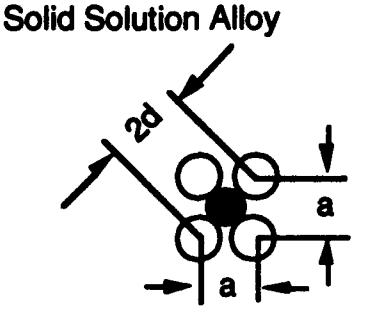

$$a^2 + a^2 = [(1-X_{Mo})2r_{Al} + (X_{Mo})2r_{Mo}]^2$$

$$a = \sqrt{2}\,[(1-X_{Mo})2.86 + (X_{Mo})2.72]$$

Where: X = Atomic Fraction Molybdenum

Figure 25. ***Geometric Schematic Illustrating the Relationship Between Lattice Parameter and Atomic Fraction Solid Solution Molybdenum in Aluminum.***

By solid solution substitution of the smaller molybdenum atom in the aluminum face center cubic lattice, the lattice parameter can be calculated by the following:

$$a^2 + a^2 = [(1-X_{Mo})2r_{Al} + (X_{Mo})2r_{Mo}]^2$$

$$a = \sqrt{2}[(1-X_{Mo})2.86 + (X_{Mo})2.72]$$

where X is the atomic fraction of molybdenum in solid solution in the face center cubic lattice. Using this relationship, 17.5 atomic percent Mo in the alloy on the Gr fibers was calculated which correlates well with the 17 atomic percent Mo measured using EDS.

Fiber Consolidation

A diffusion bonding consolidation tool has been machined from 304 stainless steel with a 2.54 x 7.62 cm cavity area. Key parameters for the consolidation study of temperature and pressure are listed in the test matrix in Table 3. Based on the hardness values determined earlier[7] which indicated that the Al-Mo alloys have a flow strength of ~ 2X high strength aluminum, a much higher pressure may be required as compared to traditional Al matrix materials.

Nonequilibrium Mg Alloys

Initially, several nonequilibrium Mg alloys, including Mg-Cr, Mg-Y, Mg-Mo, Mg-Ta, and Mg-W, were fabricated by magnetron co-sputter deposition and tested to determine their corrosion properties. From this testing, it became evident that alloying additions of yttrium demonstrated enhanced corrosion behavior when compared to pure Mg or any of our other Mg alloys. A total of six Mg-Y alloys (ranging from 7.5 to 25.4 At. %) were fabricated for corrosion testing and alloy characterization. Anodic polarization, galvanic testing, and potentiostatic testing have all been conducted for corrosion analysis. XRD and microscopy were used for alloy characterization.

Anodic potentiodynamic polarization experiments of the Mg-Y alloys conducted in 0.1M NaCl adjusted to a pH value of 8 revealed slightly better corrosion behavior when compared to pure Mg and a commercially available WE43 alloy (Mg-3.75-4.25wt. %Y-2-2.5 wt. %Nd-0.75-1.25 wt. %heavy rare earth) (Figure 26) while the same experiments conducted in pH 12 solution showed dramatically enhanced polarization behavior (Figure 27). Polarization behavior similar to that of the pH 8 results was observed when raising the solution pH to 10. Unlike the pH 8 and 10 results, breakdown potentials observed at pH 12 were quite varied (but still well above E_{corr} for pure Mg - no passivity was observed for pure Mg or WE43). The cause for this variability is still being investigated but is believed to be related to defects. While conducting potentiostatic tests in 0.1 M Cl^- solution buffered to a pH of 12 (by mixing 500 ml of 0.05 M $Na_2HPO_4 \cdot 7H_2O$ and 269 ml of 0.1 M NaOH and diluting to 1 L using deionized water), it became clear that film defects played an important

Table 3. ***Diffusion Bonding Test Matrix for the Al-17Mo Alloy Coated Fibers.***

	Number of Diffusion Bonding Trials		
Pres. / Time	8	15	20
60	1	1	1
120	1	1	1
240	1	1	1

- Temperature = 500°C and 550°C
- Time in Minutes
- Pressure in ksi (10^3 psi)
- Repeat experiment using 3 most promising conditions

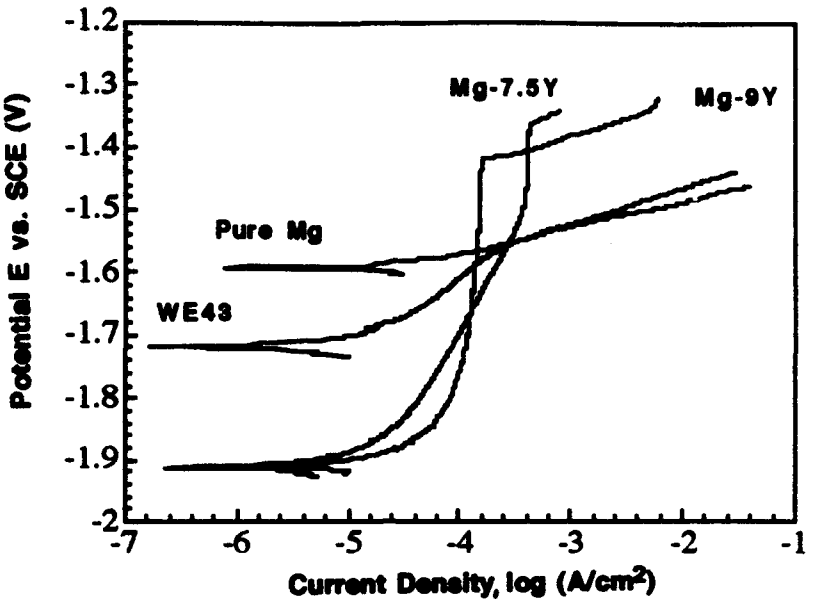

Figure 26. Comparison of Anodic Polarization Behavior for Pure Mg, WE43, and Several MgY Alloys Generated in 0.1 M NaCl (pH = 8) at a Scan Rate of 0.2 mV/s.

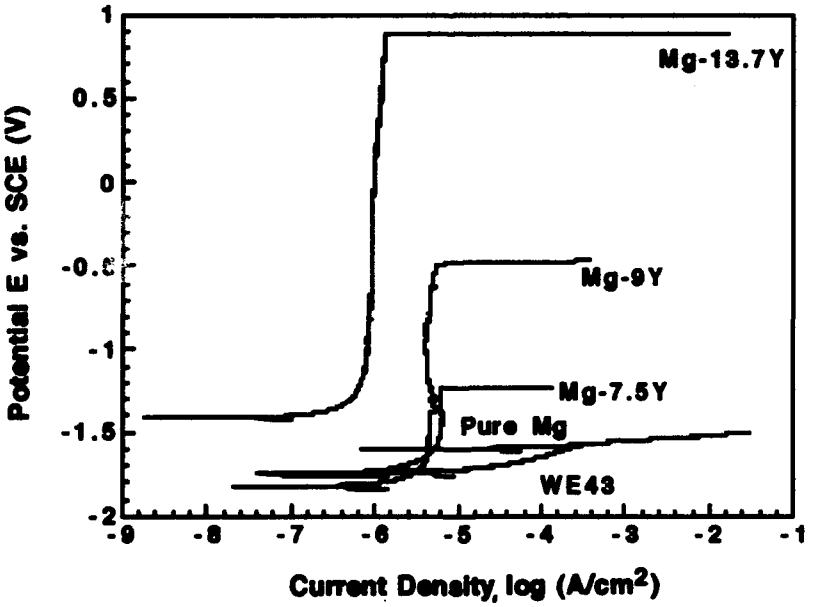

Figure 27. Comparison of Anodic Polarization Behavior for Several Mg-Y Alloys, Pure Mg, and WE43 in 0.1 M NaCl (pH = 12) Scanned at a Rate of 0.2 mV/s.

role in the quality of the alloy. Approximately 33 % of the potentiostatic tests were stopped immediately due to corrosion of the alloy occurring upon immersion in the 0.1 M Cl^- solution. It is believed that corrosion initiated at defects (either inherent or caused by handling), such as the ones shown in Figures 28 and 29, in the alloy film.[5,6] Those tests which were not terminated due to defects demonstrated promising results with one alloy exhibiting a current of 0.5 μA at a potential of +300 mV_{SCE}. Galvanic testing (coupling the Mg alloys to P75-Gr) revealed that, over a period of time, the pH of the NaCl solution was dropping significantly, causing rapid corrosion in the tests conducted in pH 12 solution. All galvanic tests conducted in pH 8 solution began corroding immediately upon coupling of the alloy with graphite. Therefore, a 0.1 M Cl^- solution buffered to pH 12 was used to determine whether the changing pH was affecting the results and the graphite area was decreased to simulate a small exposure of graphite fiber in a metal matrix composite. The alloys tested in the buffered solution exhibited much better corrosion behavior with one alloy (Mg-13.7Y) lasting for 6 days.

XRD was conducted on the sputtered Mg-Y alloys to determine whether the yttrium was in solid solution with the Mg or in the form of Mg_xY_y precipitates. Figure 30 shows XRD patterns for several Mg-Y alloys with the concentration of Y decreasing moving down the Figure. As can be seen, the two lower solute composition alloys have very sharp peaks, indicating a crystalline structure, whereas, the alloys with higher compositions have very broad peak, denoting a nanocrystalline and/or amorphous structure. The primary peak present in the crystalline alloys was at approximately 34° and was indexed to the (002) plane of Mg. The sharp peak observed at 55.5° is for the oriented Si wafer. These patterns do not correlate to the relative peak intensities of polycrystalline Mg, indicating that the sputter deposited film has preferentially grown on the Si wafer. The broad peaks observed for the higher concentration alloys were centered at 33.6° and 33.3° for Mg-20.6Y and Mg-25.4Y, respectively.

XPS was conducted on one of the alloys (Mg-22Y) to determine some of the surface characteristics of the alloy. Figure 31 is a plot showing elemental, oxide and total Mg/Y ratios (representing the integrated intensities (i.e., areas) for the respective characteristic photoelectron peaks) for the alloy. The Mg/Y (total) ratio indicated a greater amount of Mg only in the "as-received" material. Once the Mg-22Y was placed in 0.1 M NaCl solution, this ratio dropped dramatically, indicating a large increase in Y in both elemental and oxide forms. For the elemental Mg/Y ratio, a less dramatic effect was observed in going from "as-received" to pH 12 at E_{corr} and a greater change was noted in going from "as-received" to pH 8 at E_{corr}. When analyzing the data for the elemental Mg/Y ratios at a potential 400 mV anodic to E_{corr}, no elemental Mg was found. The dramatic decreases in Mg in total, oxide, and elemental could indicate several things. First, upon immersion, the Mg could have gone into solution, creating a Y-enriched layer at the surface of the alloy. Second, the oxide layer may have grown sufficiently enough so that the XPS did not detect the elemental Mg. Finally, significant Y-enrichment in the passive film could have occurred. Analysis of one of the as-sputtered data sets did not yield good information regarding the Mg/Y oxide and elemental ratios and therefore was not plotted.

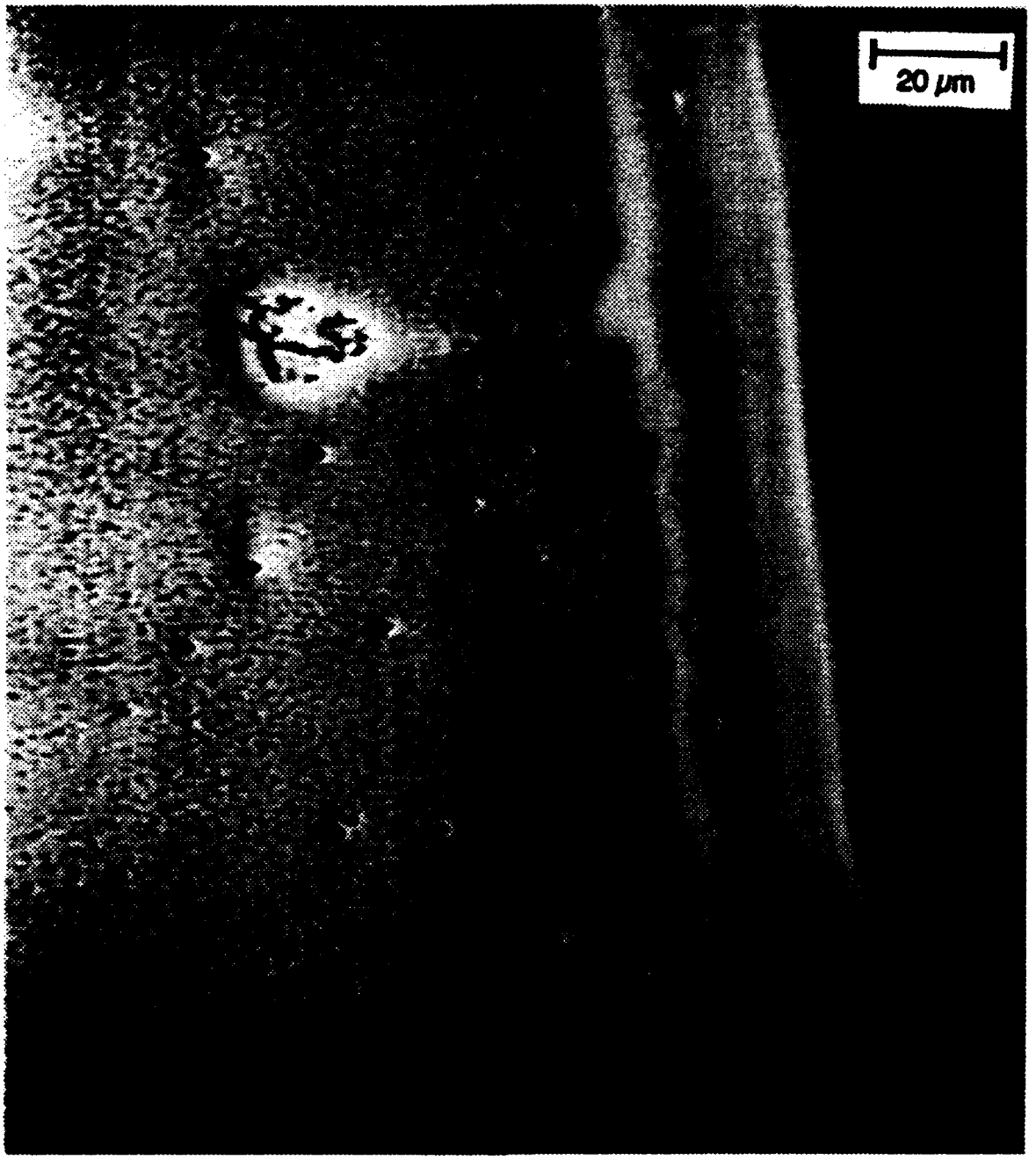

Figure 28. ***SLM Micrograph Showing Defects on the Surface of an Uncleaved, Untested Mg-25Y Alloy.***

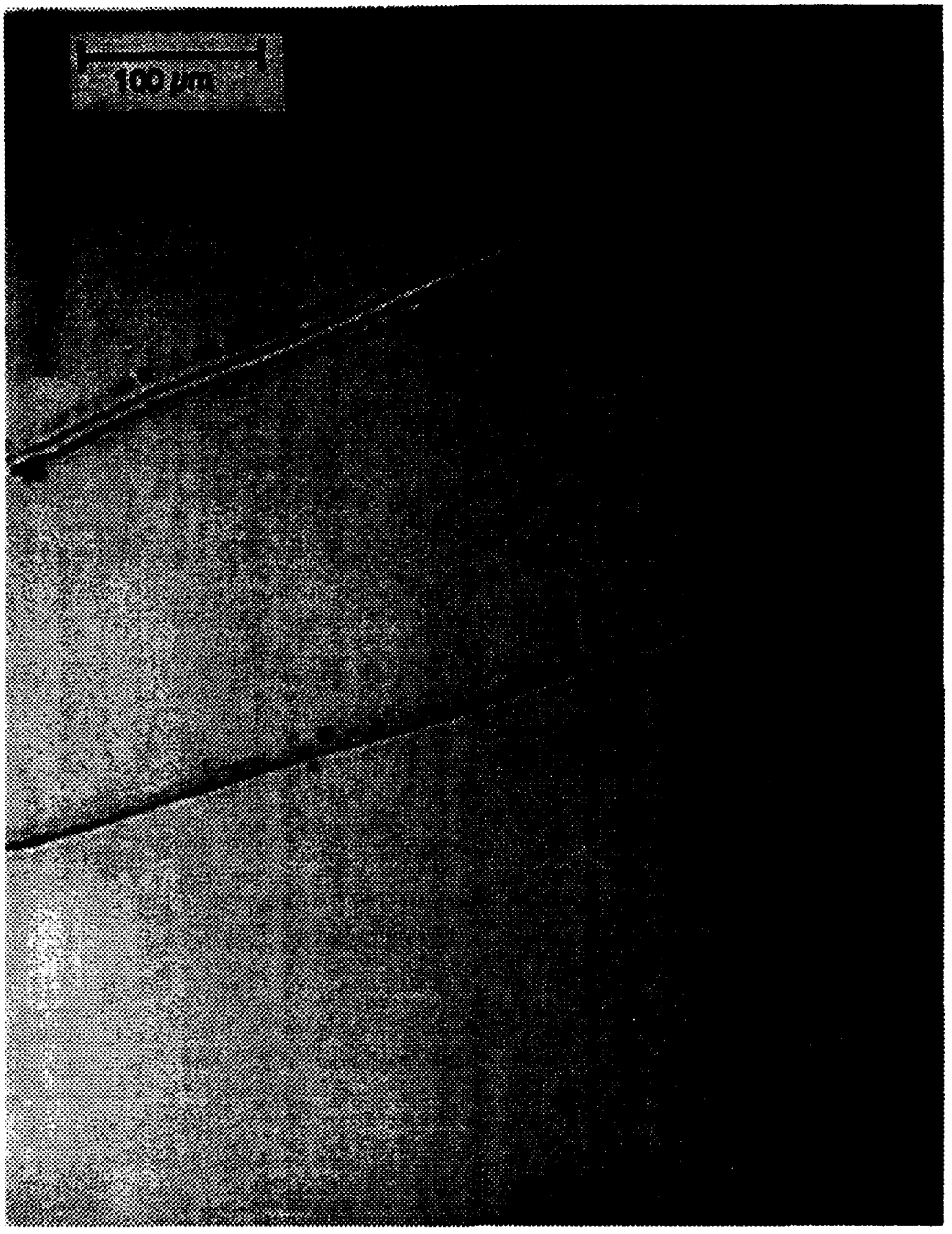

Figure 29. ***SLM Micrograph Showing Two Scratches on the Surface of an Uncleaved, Untested Mg-14Y Alloy.***

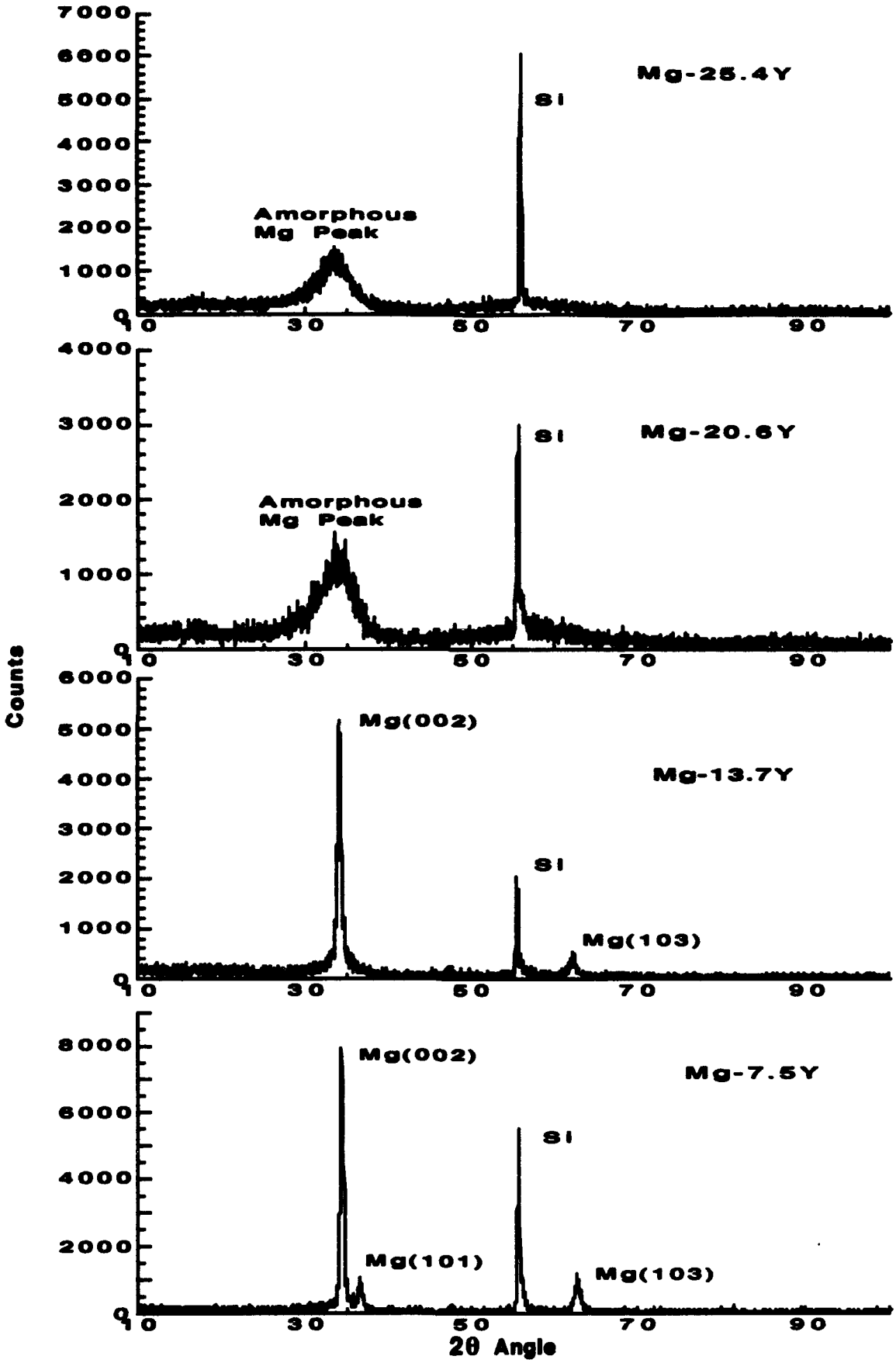

Figure 30. XRD Patterns for Four of the MgY Alloys. Solute Concentration Decreases Moving Down the Figure.

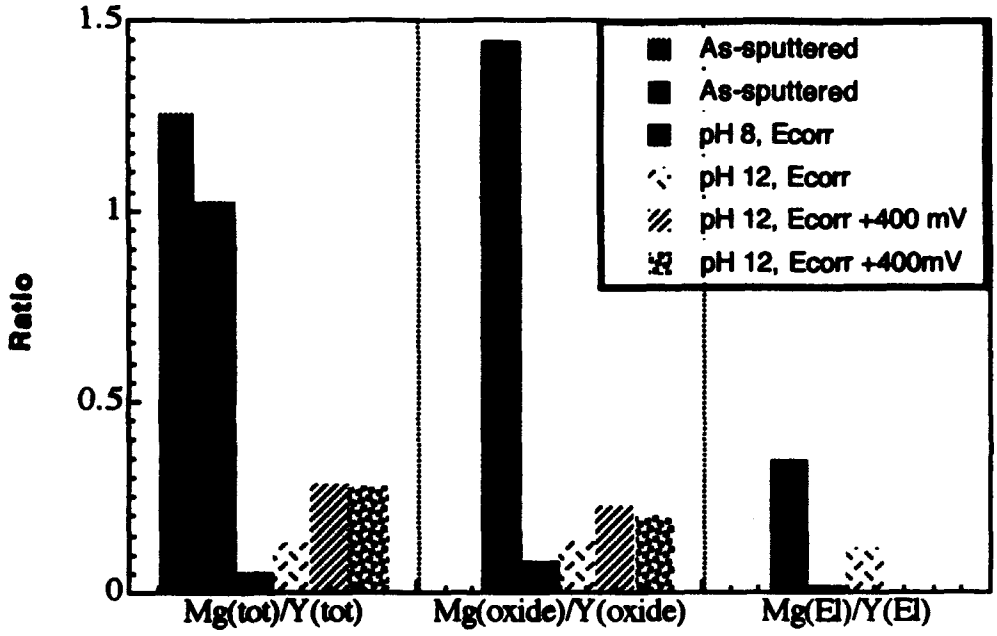

Figure 31. ***Plot of Mg/Y Elemental, Oxide, and Total Ratios Obtained from XPS Analysis. A Decrease in Height of a Bar Indicates an Increase in Yttrium Content.***

Inhibitive Surface Treatments

As an expansion of the original program, we investigated the use of inhibitive surface treatments for enhancing the corrosion resistance of Mg and Mg-based composites. Earlier research conducted by Mansfeld *et. al.*[12] with Al, was used as the basis for our research. Table 4 shows the treatments we have evaluated to date for Mg. Inhibitors which, thus far, have demonstrated the best improvements in the anodic polarization behavior of Mg are: (1) immersion in 0.01 M cerium nitrate (pH 10) for 4 hrs at 60 - 70 °C followed by polarization in 0.1 M sodium molybdate (pH 12) in the passive region at room temperature for 2 hrs, and (2) immersion in 0.01 M yttrium nitrate (pH 4.6) for 4 hours at a temperature of 60 - 70 °C. Figure 32 shows anodic polarization curves for Mg in a 0.1 M chloride solution following these treatments. For aluminum, the inhibitive treatment consisting of immersion in 0.01 M $Ce(NO_3)_3$ (pH 3.4) for 2 hrs followed by immersion in 0.005 M $CeCl_3$ (pH 5.5) for 2 hours followed by polarization in 0.1 M sodium molybdate (pH 7) at a potential of -1 V_{SCE} for 2 hrs, resulted in the polarization behavior shown in Figure 33. While the improvements noted for the Mg substrate are not nearly as good as those observed for Al, the positive shift in E_{corr} (resulting from the inhibitive treatment) could significantly reduce the corrosion of Mg in a galvanic couple. Based on the results of the thin-film work, we have recently initiated some experiments using a yttrium treatment which has also shown promise of increasing the corrosion resistance of Mg. Recent experiments using CeF_3 have also shown some promise of enhancing the polarization behavior of Mg.

Table 2. Surface Inhibitive Treatments Evaluated Tests thus far for Mg and Al.

Solution	Conc (M)	Time (hr)	Temp (°C)	pH	Solution	Conc (M)	Time (hr)	Temp (°C)	pH	Other
Magnesium										
$Ce(NO_3)_3$	0.005	2	60 - 70	3.4	$CeCl_3$	0.005	2	60 - 70	5.5	*
$Ce(NO_3)_3$	0.005	2	60 - 70	3.4						*
$Ce(NO_3)_3$	0.005	4	60 - 70	3.4						*
$Ce(NO_3)_3$	0.005	4	60 - 70	12						*
$Ce(NO_3)_3$	0.005	4	60 - 70	10						*
$Ce(NO_3)_3$	0.002	4	60 - 70	3.4						*
$Ce(NO_3)_3$	0.010	4	60 - 70	3.4						*
$Ce(NO_3)_3$	0.010	4	60 - 70	10						*
$Ce(NO_3)_3$	0.010	4	60 - 70	10						**
$Ce(NO_3)_3$	0.010	4	100	3.4						
$Ce(NO_3)_3$	0.010	4	100	10						
$Ce(NO_3)_3$	0.010	4	100	10						*
$Y(NO_3)_3$	0.010	2	60 - 70	4.6						
$Y(NO_3)_3$	0.010	2	100	4.6						
$Y(NO_3)_3$	0.010	2	room	4.6						
$Y(NO_3)_3$	0.005	2	60 - 70	4.6						
$Y(NO_3)_3$	0.010	4	60 - 70	4.6						
$Ce(NO_3)_3$	0.010	2	60 - 70	10	$Y(NO_3)_3$	0.010	2	60 - 70	4.6	
$Y(NO_3)_3$	0.010	2	60 - 70	4.6	$Ce(NO_3)_3$	0.010	2	60 - 70	10	
CeF_3	0.005	2	60 - 70	5.6						
CeF_3	0.005	2	room	5.6						
CeF_3	0.005	2	100	5.6						
CeF_3	0.001	2	60 - 70	5.6						
CeF_3	0.001	4	60 - 70	5.6						
CeF_3	0.001	2	60 - 70	12						
CeF_3	0.001	2	60 - 70	5.6	$Ce(NO_3)_3$	0.010	2	100	10	
$Ce(NO_3)_3$	0.010	2	100	10	CeF_3	0.001	2	60-70	5.6	
$Ce(NO_3)_3$	0.010	2	100	10	CeF_3	0.001	2	60-70	5.6	*
CeF_3	0.001	4	60 - 70	5.6						*
Aluminum										
$Ce(NO_3)_3$	0.005	2	room	3.4						
$Ce(NO_3)_3$	0.005	2	60 - 70	3.4						
$Ce(NO_3)_3$	0.005	2	100	3.4						
$Ce(NO_3)_3$	0.010	2	100	3.4						
$Ce(NO_3)_3$	0.010	2	100	6						
$Ce(NO_3)_3$	0.010	4	100	6						

* Sample was then immersed in 0.1 M Na_2MoO_4 (pH 12) and held at a potential in the passive region for 2 hours.
** Sample was then immersed in 0.1 M Na_2MoO_4 (pH 10) and held at a potential in the passive region for 2 hours.
***Sample was then immersed in 0.1 M Na_2MoO_4 (pH 7) and held at a potential in the passive region for 2 hours.

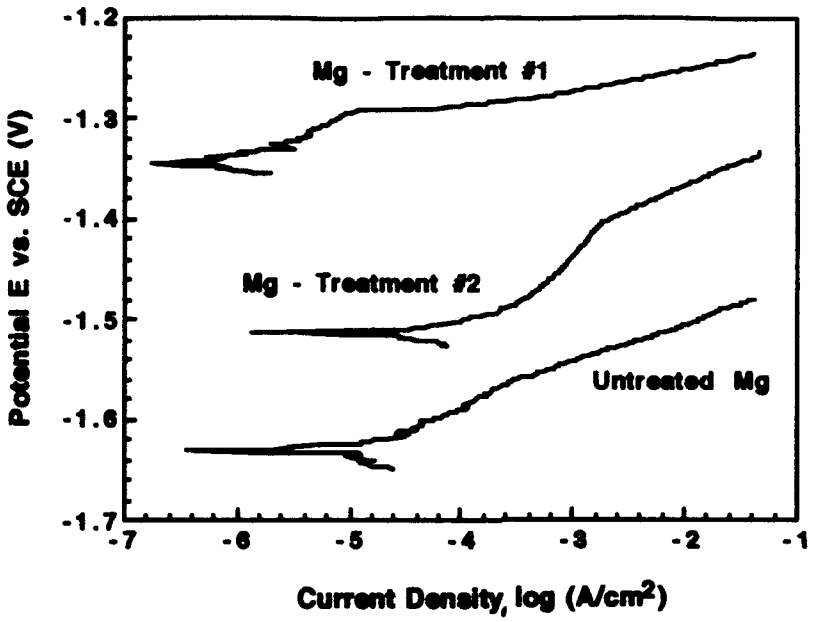

Figure 32. Anodic Polarization Behavior for Untreated Mg, Mg Treated in 10 mM $Ce(NO_3)_3$ (pH = 10) for 4 hrs at 60 to 70 °C Followed by Immersion in 0.1 M Na_2MoO_4 (pH = 12) and Holding the Mg at a Potential in the Passive Region for 2 hrs [Treatment #1], and Mg Treated in 10 mM $Y(NO_3)_3$ (pH = 4.6) for 4 hrs at a Temperature of 60 - 70 °C [Treatment #2]. Polarization Curves were Generated at a Scan Rate of 0.2 mV/s in 0.1 M NaCl Solution (pH = 8).

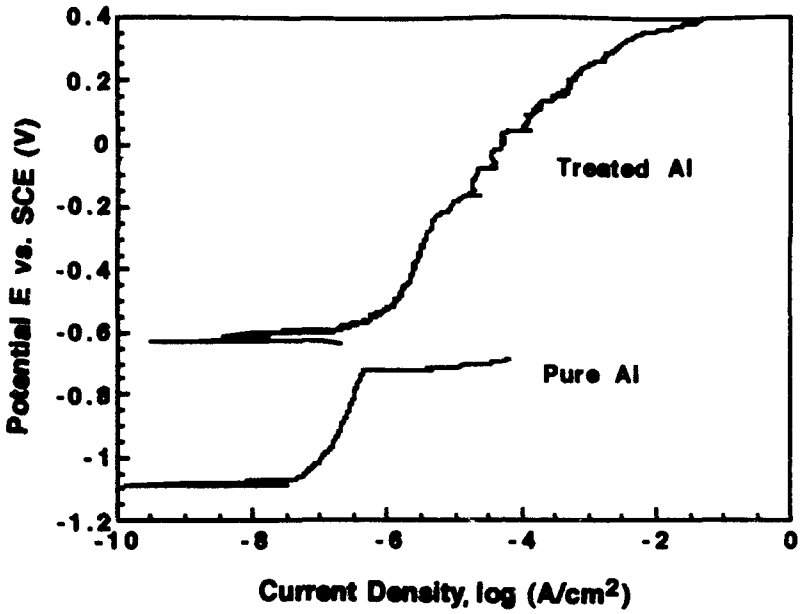

Figure 33. ***Comparison of Anodic Polarization Behavior for Pure Al Untreated and Pure Al Treated for 2 hrs in 10 mM $Ce(NO_3)_3$ (pH = 3.4) at 100 °C Followed by 2 hrs in 5 mM $CeCl_3$ (pH = 5.5) at 100 °C Followed by Immersion in 0.1 M Na_2MoO_4 (pH = 7) and Holding the Al at a Potential in the Passive Region for 2 hrs. Polarization Testing was Conducted in 0.1 M NaCl (pH = 8) at a Scan Rate of 0.2 mV/s.***

Summary

Sputter-deposited nonequilibrium Al and Mg alloys have been shown to exhibit significantly increased corrosion resistance when compared to their pure counterparts. XRD of the as-deposited Al-Mo and Mg-Y alloys revealed no second phase precipitates. Heat treatment of Al, containing 18 to 23 % Mo, revealed no precipitation at temperatures up to 400 °C for periods of up to 8 hrs and these alloys exhibited corrosion behavior similar to the as-deposited alloys. TEM was conducted on the Al-18Mo and revealed that no precipitates were present when the alloy was heat-treated at 400 °C (for up to 8 hrs) but that heat treatment at 500 °C for 1 hr or longer resulted in the formation of precipitates.

Successful fiber coating with Al, containing 15 - 18 % Mo, was accomplished using a planar cathode configuration. XRD of these coated fibers revealed that Mo was in solid solution with Al and that both amorphous and crystalline Al-Mo were present.

Breakdown potentials were quite varied for the Mg-Y tested in pH 12 0.1 M NaCl, while smaller differences were noted for the Al and lower pH Mg alloys. These variations in E_b for both alloys appear to be the result of defects such as pinholes, scratches and dust inclusions caused by both the sputter process and handling of the thin-film alloys.

XPS of Mg-22Y revealed that, once immersed in Cl^- solution, yttrium became enhanced in both oxidized and elemental forms. This Y-enhanced oxide film was believed to be a major contributor in the significantly enhanced corrosion resistance observed in the high pH solution.

Inhibitive treatments on pure Mg revealed small increases in corrosion resistance and positive shifts in E_{corr} when compared to untreated Mg, while treatments for the pure Al resulted in significantly greater corrosion resistance and also a positive shift in E_{corr}. While the improvements noted for the Mg substrate are not as good as those observed for Al, positive shifts in E_{corr} could significantly reduce the corrosion of Mg in a galvanic couple.

As a result of this year's work, one paper has been published and one has been accepted for publication (both in *Corrosion* Journal). These papers are presented in appendices 1 and 2.

References

1. D.M. Aylor and R.M. Kain, ASTM STP864 - Recent Advances in Composites in the US and Japan, Vinson and Taya (editors), American Society for Testing and Materials, Philadelphia, 632 (1985).

2. W.H. Pfeifer, W.J. Renton (editor), American Institute of Aeronautics and Astronautics, New York 231 (1977).

3. M.G. Vassilaros, D.A. Davis, G.L. Steckel, and J.P. Gudas, Proceedings of the 1980 Tri-Service Corrosion Conference, Vol. 2, US Government Publication, 21 (1980).

4. P.P. Trzaskoma, "Corrosion Behavior of Graphite Fiber/Magnesium Metal Matrix Composites in Aqueous Chloride Solution," *Corrosion*, **42**, 609 (1986).

5. E. Chin and J. Nunis, Advances in Magnesium Alloys and Composites, Paris and Hunt (editors), The Minerals, Metals, and Materials Society (1980).

6. T.R. Schrecengost, M.S. Thesis, The Pennsylvania State University (1992).

7. R.G. Wendt, M.S. Thesis, Colorado School of Mines (1993)

8. P.L. Miller, M.S. Thesis, The Pennsylvania State University (1994).

9. P.L. Miller, B.A. Shaw, R.G. Wendt, and W.C. Moshier, "Technical Note: Improving Corrosion Resistance of Magnesium by Nonequilibrium Alloying with Yttrium," *Corrosion*, **49**, 947 (1993).

10. T.R. Schrecengost, B.A. Shaw, R.G. Wendt, and W.C. Moshier, "Nonequilibrium Alloying of Graphite-Reinforced Aluminum Metal Matrix Composites," *Corrosion*, **49**, 842 (1993).

11. B.D. Cullity, Elements of X-ray Diffraction, 2nd Edition, Addison-Wesley Publishing Co., Philippines, 87 (1978).

12. F. Mansfeld, Y. Wang, and H. Shih, "Steps Towards a Stainless Aluminum Alloy," Dept. of Materials Science and Engineering," NACE Research in Progress Symposium 92, Cincinnati, OH (1992).

Appendix 1

Technical Note: Improving Corrosion Resistance of Magnesium by Nonequilibrium Alloying with Yttrium

Technical Note: Improving Corrosion Resistance of Magnesium by Nonequilibrium Alloying with Yttrium*

P.L. Miller, B.A. Shaw, R.G. Wendt, and W.C. Moshier***

ABSTRACT

Significant improvements were achieved in the anodic polarization behavior of magnesium (Mg) by nonequilibrium alloying with 9 at% to 22 at% yttrium (Y). Alloys were fabricated using the nonequilibrium technique of magnetron cosputter deposition. Anodic potentiodynamic polarization experiments were conducted at various scan rates and pH values to assess the corrosion resistance of several MgY alloys. These alloys exhibited significantly enhanced corrosion behavior compared to pure Mg. Differences included higher breakdown potentials and lower passive current densities. X-ray diffraction of each alloy revealed the Y was retained in solid solution.

KEY WORDS. anodic polarization, breakdown potential, corrosion resistance, magnesium, nonequilibrium alloying, pH, x-ray diffraction, yttrium

INTRODUCTION

Previous researchers have reported that alloying additions of yttrium (Y) to magnesium (Mg) enhanced castability and improved its corrosion resistance modestly.[1-3] Unsworth and King documented that an alloy of Mg, Y, and neodymium (Nd) exhibited increased corrosion resistance and better overall castability compared to other Mg alloys.[1] One concern associated with this research was the presence of precipitates in the Unsworth and King alloy. Second phases increase susceptibility of Mg to galvanic corrosion. Since Mg is extremely electrochemically active, microgalvanic cells could have been established between the Mg and any other phases present. In addition, the formation of precipitates may have tied up the Y, preventing it from contributing to passive film formation.

Krishnamurthy, et al., noted a pseudopassive behavior in rapidly solidified Mg alloys containing 15 wt% to 26 wt% Y.[2] These alloys exhibited a large active nose in the polarization curves prior to formation of the pseudopassive film at relatively high potentials (from 500 mV_{SCE} to more than 1,000 mV_{SCE}). Current densities of a few hundred $\mu A/cm^2$ were observed in the pseudopassive region. Since enhanced passivity was not observed for ingot alloys with the same composition, Krishnamurthy, et al., attributed the improved polarization behavior to the more homogeneous and refined microstructures obtained through rapid solidification of the alloys. While these results showed promise for improving the corrosion resistance of Mg with the addition Y, the large active nose in the polarization curve at the open-circuit potential (E_{oc}) was a significant concern.

Retaining Y in solid solution with Mg is an important step in enhancing the MgY alloy's corrosion behavior. Of the melt spun ribbons tested by Krishnamurthy, the Mg-15 at% Y and Mg-20 at% Y both contained Y-rich precipitates, while the Mg-26 at% Y displayed a "martensitic" type of structure without precipitates.[2] Based on the MgY binary phase

* Submitted for publication August 1993; in revised form, October 1993.
* Pennsylvania State University, University Park, PA 16802.
** Martin Marietta Astronautics Group, Denver, CO 80201

0010-9312/93/000223/$3.00/0
NACE International

diagram. Y alloying additions have a limited solubility (3.75 at%) in Mg.[3]

Magnetron cosputter deposition is a nonequilibrium alloying technique which has been shown to increase the amount of solute that can be maintained in solid solution.[5,18] The objective of this study was to investigate the corrosion behavior of several MgY alloys made by this nonequilibrium alloying technique.

EXPERIMENTAL

MgY alloys were fabricated using magnetron cosputter deposition. Two targets, pure Mg (99.95%) and pure Y (99.95%), were sputtered onto single crystal silicon (Si) substrates, yielding a MgY film ~ 2 μm thick. The substrate was rotated at 30 rpm to ensure uniform solute concentration across the alloy films. Two alloys, Mg-9 at% Y and Mg-22 at% Y, were fabricated for evaluation and testing. Y concentrations in the alloys were estimated using semiquantitative energy dispersive spectroscopy (EDS). Alloys were characterized using x-ray diffraction (XRD), which confirmed that Y solute was retained in solid solution with Mg after the sputtering process.

Specimens for corrosion testing were fabricated by cleaving the alloy-coated Si wafer into 16 pieces, each with an area of ~ 4 cm^2 to 5 cm^2. Individual pieces were then coupled to a potentiostat through a lead wire. Except for the test area, all regions were coated with an adherent marine epoxy to ensure that environmental and electrical isolation were maintained. Anodic potentiodynamic polarization of all alloys was performed using a conventional three-electrode technique on a potentiostat interfaced with a personal computer. All testing was conducted at ambient lab temperature (~ 25°C) in quiescent, 0.1 M sodium chloride (NaCl) solution at pH values of 8, 10, and 12, adjusted using dilute sodium hydroxide (NaOH). All reported potential values were referenced to a saturated calomel reference electrode (SCE). The anodic scans were generated at 0.2 mV/s and 0.05 mV/s. At least two anodic polarization curves were generated for each condition. Prior to anodic polarization, E_{oc} were allowed to stabilize for approximately 30 min. The data were corrected for impedance resistance (IR) drop every 10 s using the current interrupt feature of the potentiostat.

RESULTS AND DISCUSSION

Figure 1 shows anodic polarization curves for Mg, Mg-9 at% Y, Mg-22 at% Y, and Y, generated at a scan rate of 0.2 mV/s in 0.1 M NaCl at pH = 8. Polarization curves for Mg were generated using wrought Mg (99.95%), while sputtered films were used for the Y

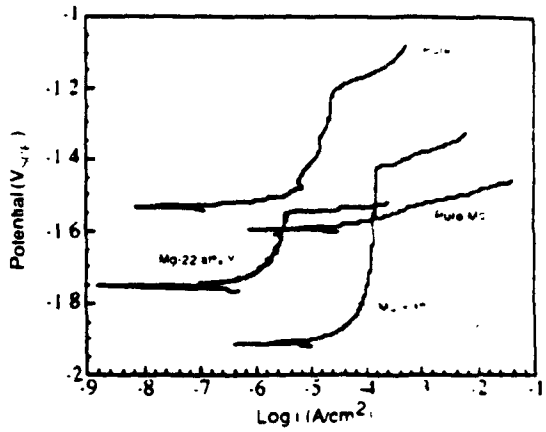

FIGURE 1. *Anodic potentiodynamic polarization curves for Mg, Mg-9 at% Y, Mg-22 at% Y, and Y generated at a scan rate of 0.2 mV/s in 0.1 M NaCl, pH 8, 25 C*

and MgY alloys. Sputtered Mg was not used because of its extremely rapid degradation in atmosphere and in solution. The only notable difference between wrought and sputtered Mg was E_{oc}, which for wrought Mg ranged from −1,560 mV_{SCE} to −1,590 mV_{SCE}. E_{oc} values for sputtered Mg were 120 mV_{SCE} to 140 mV_{SCE} more electrochemically active than those of wrought Mg. More active E_{oc} values for the sputtered Mg were believed to result from impurities going into solid solution with the Mg and from finer grain sizes incurred during the deposition process. At pH = 8, the Mg-22 at% Y maintained a lower passive current density (i_{pass}), whereas the Mg-9 at% alloy displayed the higher breakdown potential (E_b). Values for i_{pass} ranged from 0.7 A/cm^2 to 4.9 A/cm^2 for Mg-22 at% Y. Values for Mg-9 at%Y were between 40 μA/cm^2 and 128 μA/cm^2. E_b values for Mg-9 at% Y ranged from −1,398 mV_{SCE} to −1,460 mV_{SCE}, whereas E_b values for Mg-22 at% Y were between −1,543 mV_{SCE} and −1,597 mV_{SCE}. E_{oc} for both alloys decreased with the addition of Y to Mg. Lower E_{oc} values for the MgY alloys compared to pure Mg probably resulted from differences in Tafel behavior and exchange current density (i_o). Mg exhibited an i_o value (10^{-6} A/cm^2 to 10^{-9} A/cm^2) greater than that of Y (10^{-9} A/cm^2 to 10^{-12} A/cm^2).[19]

Experimental data revealed i_o values of 10^{-7} A/cm^2 to 10^{-7} A/cm^2 for Mg and 10^{-9} A/cm^2 for Y. The data were consistent with results reported by West.[19] Therefore, a lower E_{oc} value was obtained by alloying Mg with Y. These trends also applied to anodic polarization curves generated at the scan rate of 0.05 mV/s. The slower scan rate curves were generated to ensure that decreasing the scan rate did not affect E_b significantly.

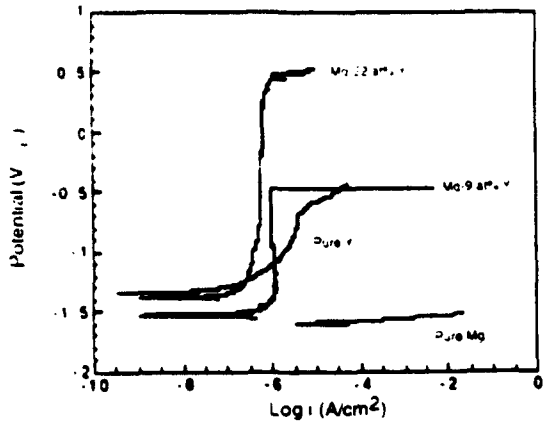

FIGURE 2. *Anodic potentiodynamic polarization curves for Mg, Mg-9 at% Y, Mg-22 at% Y, and Y generated at a scan rate of 0.05 mV/s in 0.1 M NaCl, pH 12, 25°C.*

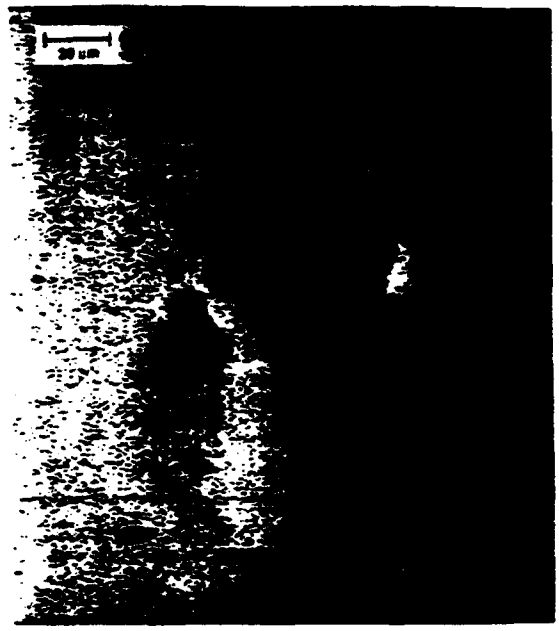

FIGURE 3. *Scanning laser microscope photo of an uncleaved, untested MgY alloy showing disparities on the surface (950x).*

Based on thermodynamic behavior alone, Mg might be expected to have better corrosion resistance at pH values above ~ 11.6.[20] Increasing the solution pH from 8 to 10 yielded little change in the anodic polarization behavior of the MgY alloys. The only notable difference was an increase in E_o (approximately 100 mV_{SCE}) for the Mg-22 at% Y alloy. Compared to that of pure Mg, anodic polarization curves for MgY alloys generated at pH values of 8 and 10 exhibited increased corrosion resistance. Changing solution pH from 10 to 12 resulted in significant changes in the polarization behavior of the MgY alloys.

Figure 2 shows anodic polarization curves for pure Mg, Mg-9 at% Y, Mg-22 at% Y, and pure Y generated at a scan rate of 0.05 mV/s in 0.1 M NaCl, pH = 12. Values of i_{pass} for the Mg-22 at% Y alloys were slightly lower (0.5 μA/cm²) than those of the Mg-9 at% Y alloys (1.3 μA/cm²). E_{oc} values were more electro-chemically noble in the pH 12 solution, compared to values observed at pH 8 and 10. Values of E_o for both alloys tested at pH 12 varied from –465 mV_{SCE} to –972 mV_{SCE} for Mg-9 at% Y and +340 mV_{SCE} to –92 mV_{SCE} for the Mg-22 at% Y alloy. The wide range of E_o values was believed to be a result of film defects, such as the one shown in Figure 3, created during the sputtering and handling processes.[3] Another possibility for the varied E_o values was that the 0.05 mV/s scan rate used for the anodic potentiodynamic curves was not slow enough to allow electrolyte-film surface reactions to reach steady state. In contrast to the anodic polarization curves generated at a pH of 8, E_o at a pH of 12 for the alloy containing higher concentrations of Y was consistently greater than that of Mg-9 at% Y.

Krishnamurthy, et al., conducted anodic potentiodynamic polarization experiments with Mg-Y (approximately 5 at% to 9 at%) in 0.01 M NaCl (pH not mentioned) and found that ribbons and splats exhibited a pseudopassive behavior at high potentials (> 250 mV_{SCE}), which led to lower current densities of 300 μA/cm² to 400 μA/cm².[2] Comparing those pseudopassive current densities to those obtained in the present work, much lower passive current densities were observed for the sputterdeposited alloys tested in a higher (0.1 M) concentration NaCl solution.

Pseudopassive behavior of Krishnamurthy's alloys at such high overpotentials may be unrealistic in most practical applications. At low to moderate overpotentials, the sputterdeposited MgY alloys exhibited significantly lower current densities compared to the splat-quenched alloys. The enhanced corrosion resistance obtained for the sputter-deposited alloys likely resulted from the absence of second phases, which freed more Y solute to be used for passivity enhancement of the alloy.

CONCLUSIONS

- Addition of Y to Mg significantly altered its polarization behavior. Differences included increased E_o and lower i_{pass} values compared to pure Mg.

- Both MgY alloys exhibited greater corrosion resistance than pure Mg when tested in 0.1 M NaCl solution at pH =12. These results were a dramatic improvement in both E_o and i_{pass} for Mg alloys. Values for E_o were quite varied at the high pH for both scan rates. Even with the wide variability in E_o noted for the low-solute-concentration alloy, this polarization behavior represented a significant improvement over pure Mg and other Mg alloys.

ACKNOWLEDGMENTS

The authors acknowledge the support of A.J. Sedriks of the U.S. Office of Naval Research. This project was funded by the ONR under contract number N00014-91-J-1196.

REFERENCES

1. W. Unsworth, J. King, Metallurgia 53 (1986): p. 199.
2. S. Krishnamurthy, M. Khobaib, E. Robertson, F.H. Froes, Mater. Sci. E. 99 (1988): p. 507.
3. A. Joshi, R.E. Lewis, Advances in Magnesium Alloys and Composites, H. Paris, W.C. Hunt, eds., 95 (Warrendale, PA: TMS, 1988).
4. T.B. Massalski, ed., Binary Alloy Phase Diagrams, 2nd ed., Vol. 3 (Metals Park, OH: ASM International, 1990): p. 2,568.
5. T.R. Schrecengost, B.A. Shaw, R.G. Wendt, W.C. Mosher, Corrosion 43 (1993): p. 842.
6. R.G. Wendt, Development of Corrosion Resistant Aluminum Alloys for Graphite Fiber Composites (Master's thesis, Colorado School of Mines, 1992).
7. W.C. Mosher, G.D. Davis, J.S. Ansearn, H.F. Hough, J. Electrochem. Soc. 133 (1986): p. 1,063.
8. W.C. Mosher, G.D. Davis, J.S. Ansearn, H.F. Hough, J. Electrochem. Soc. 134 (1987): p. 2,677.
9. W.C. Mosher, G.D. Davis, G.O. Cote, J. Electrochem. Soc. 136 (1989): p. 356.
10. G.D. Davis, W.C. Mosher, T.L. Fritz, G.O. Cote, J. Electrochem. Soc. 137 (1990): p. 422.
11. B.A. Shaw, T.L. Fritz, G.D. Davis, W.C. Mosher, J. Electrochem. Soc. 137 (1990): p. 1,317.
12. G.D. Davis, W.C. Mosher, G.G. Long, D.R. Black, J. Electrochem. Soc. 138 (1991): p. 3,194.
13. B.A. Shaw, G.D. Davis, T.L. Fritz, B.J. Rees, W.C. Mosher, J. Electrochem. Soc. 138 (1991): p. 3,288.
14. B.A. Shaw, G.D. Davis, T.L. Fritz, B.J. Rees, W.C. Mosher, in Critical Factors in Localized Corrosion, G.S. Frankel, R.C. Newman, eds., PV 92-9, (Pennington, NJ: The Electrochemical Society Softbound Proceedings Series, 1992), p. 323.
15. G.S. Frankel, M.A. Russak, C.V. Jahnes, M. Mirzamaani, V.A. Brusic, J. Electrochem. Soc. 136 (1989): p. 1,243.
16. H. Yoshioka, H. Habazaki, A. Kawashima, K. Asami, K. Hashimoto, Corros. Sci. 32 (1991): p. 313.
17. H. Yoshioka, A. Kawashima, K. Asami, K. Hashimoto, in Corrosion Electrochemistry and Catalysis of Metallic Glasses, R.B. Diegle, K. Hashimoto, eds., PV 88-1 (Pennington, NJ: The Electrochemical Society Softbound Proceedings Series, 1988), p. 242.
18. Z. Szklarska-Smialowska, in Critical Factors in Localized Corrosion, G.S. Frankel, R.C. Newman, eds., PV 92-9, (Pennington, NJ: The Electrochemical Society Softbound Proceedings Series, 1992), p. 311.
19. J.M. West, Electrodeposition and Corrosion Processes (London, U.K.: Van Nostrand Reinhold, 1965), p. 50.
20. M. Pourbaix, Atlas of Electrochemical Equilibria in Aqueous Solutions (Houston, TX: NACE, 1974), p. 141.

Appendix 2

Corrosion Resistant Aluminum Matrix for Graphite-Aluminum Composites

Corrosion Resistant Aluminum Matrix for Graphite/Aluminum Composites

Robert G. Wendt and William C. Moshier
Martin Marietta Astronautics
Denver CO, 80201

Barbara Shaw and Paul Miller
Pennsylvania State University
University Park, PA 16802

David L. Olson
Colorado School of Mines
Golden, CO 80401

ABSTRACT

Graphite/Aluminum (Gr/Al) metal matrix composites possess several attractive mechanical and thermal properties but use of this material has been limited, in part, because it is extremely susceptible to corrosion. In this study, corrosion resistant aluminum alloys that contained non-equilibrium concentrations of molybdenum were developed as the matrix for Gr/Al composites using co-sputter deposition. Corrosion testing included potentiodynamic polarization and galvanic coupling of as-sputtered and heat treated alloys. Polarization behavior of the as-sputtered and heat treated alloys measured in NaCl solutions was found to be greatly improved over pure aluminum and traditional Gr/Al matrix alloys such as 6061 Al. Galvanic current density values for as-deposited and heat treated Al-18Mo and Al-23Mo alloys coupled to equal areas of P75 Gr fibers were measured and found to be up to three orders of magnitude lower than for pure sputtered Al-to-Gr couples. Galvanic diagrams for the Al-Mo alloys indicated corrosion was controlled by the anodic reaction irrespective of the cathode-to-anode area ratio.

1.0 INTRODUCTION

High modulus Gr/Al metal matrix composites (MMCs) offer a high specific modulus and strength (E/ρ and UTS/ρ), high thermal conductivity (K), and a coefficient of thermal expansion (α) that can be designed to be 0 $\mu m/m/^{\circ}C$ by selecting the appropriate Gr fiber type, volume, and lay-up. These properties are ideal for designing mechanically (E/ρ) and thermally (α/K) stable structures. However, Gr/Al is very susceptible to corrosion, which has severely limited its application in aircraft, spacecraft, and marine structures.

Gr/Al composites have been shown to corrode eighty times faster than monolithic Al alloys in an aerated 3.15 weight percent NaCl solution at room temperature [Ref 1]. One key factor behind the rapid corrosion of Gr/Al composites was residual microstructural chlorides introduced during the liquid metal infiltration (LMI) process used to fabricate precursor Gr/Al wires [Ref 1-4]. Corrosion of Gr/Al composites initiated by pitting of the aluminum facesheet foils at a rate commensurate with Al alloys. Once the Al facesheet foils were penetrated, corrosion was accelerated by residual microstructural chlorides within the composite and by exposure of the Gr fibers creating a galvanic couple.

To improve the corrosion resistance of Gr/Al, several techniques, including coatings, cathodic protection, and cathodic inhibitors, have been investigated [Ref 1,5]. These methods provided various levels of improved corrosion resistance but only delayed pitting and subsequent galvanic interaction between the Al matrix and Gr fiber. None of these techniques addressed the true problem, which was poor corrosion resistance of the Al matrix in chloride environments, especially when the metal was galvanically coupled to Gr fibers.

An alternate method for preparing Gr/Al composites is to deposit the Al matrix directly onto each individual Gr fiber by physical vapor deposition (PVD) [Ref 6]. The flexible alloy coated fibers are arranged in the desired orientations and consolidated by diffusion bonding. The versatility of the PVD process allows for virtually any matrix alloy to be deposited onto the Gr fibers. Advantages of the PVD process over the LMI process include: 1) eliminating fiber/matrix reactions because the composites can be consolidated well below the melting point of Al where the kinetics for aluminum carbide formation are sluggish, 2) minimizing thermal strain hysteresis due to the high strength of the sputtered alloy matrix and the smaller thermal excursion required for diffusion bonding as compared to melting, 3) providing near-net shape processing capability, and 4) eliminating residual microstructural chlorides.

Several Al-Mo alloys have been fabricated using sputtering which is similar to the PVD process used for Gr/Al composites [Ref 7-11]. These Al-Mo alloys were electrochemically tested and demonstrated to exhibit improved corrosion resistance over typical Al alloys. In this study, Al-Mo alloys were investigated to determine the feasibility of using these alloys as the matrix for Gr/Al composites. Alloys were fabricated and corrosion tested to assess whether the improvement in corrosion behavior was maintained after heat treating at typical composite consolidation temperatures. In addition, galvanic corrosion experiments were conducted to determine the electrochemical stability of Al-Mo by coupling the non-equilibrium alloys to P75 Gr fibers embedded in a non-conductive epoxy. Throughout this work, the increased

density which resulted from the addition of refractory metals to Al was always taken into consideration. This work focused on Mo additions to Al as well as investigating the impact of adding magnesium as a low density ternary element to assess whether highly noble breakdown potentials could be achieved and maintained after heat treatment.

2.0 EXPERIMENTAL PROCEDURE

Binary Al-Mo and ternary Al-Mg-Mo alloys were fabricated by co-sputtering from pure element targets onto either 100-mm-dia. silicon wafers in the case of the binary alloys or single crystal sapphire for the Al-Mg-Mo alloy. Sapphire was used for the ternary alloy to eliminate the formation of $MgSi_2$ at low temperatures and short heat treatment times. However, sapphire was also found to react with the Mg to form spinels and oxides during heat treating. Hence, it was difficult to identify an inert substrate for the ternary alloy study.

Substrate temperature was not controlled during sputtering and reached a maximum of approximately 100°C during a 1 h deposition that resulted in a ~1μm thick alloy film. Alloy composition was controlled by holding the Al cathode power constant at 485 W RF while the power to the Mo and Mg cathodes was varied between 10 and 100 W DC. High purity argon (10 parts per billion oxygen) working gas was introduced at a flow rate of 200 standard cubic centimeters per minute (SCCM) and pressure was held constant at 7.0 mtorr by adjusting the conductance of the system. The sputtering heads were spaced approximately 100 mm from the substrate focused at 60° from the substrate normal. By rotating the substrate at 30 revolutions per minute (RPM), alloy composition uniformity could be maintained to within a few atomic percent solute across the substrate.

Composition of the sputtered alloys was measured using energy dispersive spectroscopy (EDS) on a scanning electron microscope (SEM). Compositions of several specimens were also measured by inductively coupled plasma (ICP) for comparison.

X-ray diffraction (XRD) was conducted using a 12 kW rotating anode diffractometer with a monochromatic Cu-K_α x-ray source. Both as-sputtered and heat treated Al-Mo alloys were analyzed to determine whether the Mo was either in solid solution with the Al and readily available for incorporation into the passive film or whether precipitation had occurred, resulting in the formation of Al_xMo_y intermetallic compounds.

Anodic polarization tests were conducted at ambient pressure and temperature in a quiescent (non-stirred with no purge gas, i.e., neither aerated nor deaerated but in open air) 0.1M NaCl solution with the pH adjusted to 8 using reagent grade NaOH.

Alloys that exhibited enhanced corrosion behavior were prepared for additional polarization tests where the concentration of chloride in solution was varied (either 0.1 M or 0.55 M NaCl) and the solution was aerated. Using a potentiostat/galvanostat, specimens were allowed to reach a stable open circuit potential and were polarized in the anodic direction starting at a potential 10 mV_{SCE} cathodic to the open circuit potential (E_{oc}) at a rate of 0.2 $mV \cdot s^{-1}$ until breakdown occurred.

Galvanic corrosion response of the Al-Mo and Al-Mg-Mo alloys was estimated using galvanic diagrams that were constructed from the polarization data [Ref 12]. In these diagrams, the anodic data for the Al-Mo alloys and pure sputtered Al were superimposed on the cathodic curve for the P75 Gr fiber. Assuming the IR drop between the metal and Gr fibers was insignificant, there were no contributions from reverse reactions, and a uniform current distribution between the metal and graphite; the intersection of the anodic and cathodic curves was used to estimate the current present in the galvanic couple.

To confirm the galvanic diagram predictions, galvanic currents were measured by coupling either the as-sputtered or heat treated alloy specimens to P75 Gr fibers. The P75 Gr fibers were prepared for testing by embedding them into a non-conductive epoxy and electrically connecting them to a external lead. Area fractions of the exposed Gr fibers were measured using a image analyzer. Nominal cathode-to-anode area ratios ranged from 0.2 to 1.1. The alloy specimen and the P75 Gr/epoxy composite were electrically coupled and immersed in a pH 8, 0.1 M NaCl solution. Galvanic current was monitored as a function of time using a potentiostat/zero resistance ammeter (operating in the ZRA mode).

3.0 RESULTS

3.1 Alloy Fabrication and Heat Treatment

Compositions and anodic polarization results of the as-sputtered Al-Mo and Al-Mg-Mo alloys are listed Table 1. All as-sputtered alloys had a highly reflective metallic appearance after sputtering indicating low levels of oxygen contamination. After heat treating, most of the alloys retained their highly reflective appearance.

XRD revealed that all of the as-sputtered alloys were amorphous as shown in the representative pattern in Figure 1. Table 2 summarizes the XRD results of the alloys that were heat treated at 400°C, 500°C and 600°C for 1, 2, and 8 h to determine the effect of composite consolidation on the alloy structure. This table shows that as the concentration of Mo in the Al alloy increased, its propensity to form precipitates during heat treatment decreased. For example, Al-11Mo precipitated at the lowest time (1 h)

and temperature (400°C); whereas the Al-23Mo remained amorphous after being heat treated at 600°C for 2h. This result was unexpected because as the Mo concentration increases, the thermodynamic driving force for precipitation increases. Lack of precipitation indicated the kinetics for precipitation in these alloys was very sluggish. The Al-Mg-Mo alloys were also amorphous in the as-sputtered condition but were found to react at all heat treatment times and temperatures forming precipitates as well as oxides due to reaction of the Mg with the sapphire substrate.

3.3 Polarization Testing

As-Deposited Alloys -- Table 1 and Figure 2 summarize the results of the anodic polarization experiments for the binary Al-Mo and ternary Al-Mg-Mo non-equilibrium alloys in the as-sputtered condition. All the as-deposited Al-Mo alloys exhibited a extended passive region and an open circuit potential that was 500 to 600 mV more noble than pure Al. Open circuit potential values for all of the alloys were measured to be between -600 to -450 mV_{SCE} with the majority of the measured E_{oc} values ranging from -520 mV_{SCE} to -580 mV_{SCE}. There was no apparent trend in E_{oc} as a function of solute concentration for the Al-Mo alloys tested, agreeing with the previous work on Al-Mo alloys [Ref 7,8,10]. Passive current densities (i_{pass}) for the as-deposited binary Al-Mo and ternary Al-Mg-Mo alloys ranged between 0.1 and 10.0 $\mu A \cdot cm^{-2}$, but as in the case of E_{oc}, no correlation between solute concentration and i_{pass} was evident. Variations in i_{pass} were attributed to general defects, i.e., scratches, pinholes, etc., in the alloy film. Breakdown potential (E_b) values for most of the as sputtered alloys were between 100 and 500 mV_{SCE} as compared to -690 mV_{SCE} for pure Al.

Additional polarization experiments were conducted on the Al-18 Mo alloy in aerated and quiescent NaCl solutions (pH 8) with Cl^- concentrations of 0.1 and 0.55 M. Figure 3 shows that the polarization response was not significantly altered by either increasing the Cl^- concentration, by solution aeration, or both.

SEM examination and EDS analysis of a newly formed pit on the as-deposited Al-18Mo specimen immediately after polarization to the breakdown potential showed the Mo concentration had risen from 18 to 25 atomic percent in the pit. Increase in Mo in the forming pit indicates the pitting process involves the preferential dissolution of Al from the alloy, which is consistent with x-ray photoelectron spectroscopy work conducted during earlier studies [Ref 8,10].

Heat Treated Alloys -- The polarization response of as-deposited and heat treated Al-11Mo alloys is shown in Figure 4. Although the breakdown potential (E_b) for the heat treated Al-11Mo alloys decreased from ~420 mV_{SCE} (as-sputtered) to 50 mV_{SCE}, (heat treated), E_{oc} remained relatively constant at approximately -550 mV_{SCE}.

Reduction in E_b was likely the result of precipitates formed during heat treatment creating microgalvanic cells with the surrounding alloy. Conversely, i_{pass} decreased from ~1 $\mu A \cdot cm^{-2}$ for the as-deposited alloy to ~0.1 $\mu A \cdot cm^{-2}$ after heat treatment.

Both E_{oc} and E_b for the Al-18Mo alloy were not dramatically affected by heat treating up to 500°C for 2 h (Fig. 5). Similar to the Al-11Mo alloys, i_{pass} for the heat treated Al-18Mo specimens was less than that for the as-sputtered alloy, with the exception of specimen heat treated at 400°C for 1 h. No cracks or defects which may contribute to lower E_b values were found during SEM examination of the heat treated alloys.

The Al-12Mg-13Mo alloy exhibited an E_{oc} value of -580 mV_{SCE} and E_b of 55 mV_{SCE} in the as-deposited condition which is similar to the Al-Mo alloys (Fig. 6). The E_{oc} value was maintained after heat treating at 400°C for 1 h, however, heat treating the ternary alloy at longer times and higher temperatures resulted in a more active E_{oc} (approximately -800 mV_{SCE}) with no passive response during polarization.

3.4 Galvanic Corrosion Behavior

Galvanic diagrams [Ref 12] based on equal metal/Gr areas for pure Al, 6061 Al, and the Al-Mo alloys coupled to P75 Gr fibers are shown in Figure 7. This diagram estimates that the galvanic corrosion of pure sputtered and 6061 Al coupled to P75 Gr fibers was cathodically controlled with a high current density value of 12.5 $\mu A \cdot cm^{-2}$. For a cathodically controlled reaction, the cathodic curve shifts to a higher current density as the Gr-to-Al area ratio increases, which accelerates the corrosion rate of the Al matrix. Converse to pure Al, galvanic corrosion was anodically controlled for the Al-Mo alloys with an estimated galvanic current density of 1 $\mu A \cdot cm^{-2}$. For anodic controlled corrosion changing the Gr-to-Al ratio and subsequently shifting the cathodic curve to higher current density values (or anodic curve to lower current density) would not significantly change the corrosion rate for the Al-Mo alloys. This result is important because modifying the Gr fiber volume, which is a key design feature of composites to achieve specific thermal or mechanical properties, will not result in dramatic changes in the corrosion response of the Gr/Al-Mo composite.

Galvanic corrosion reaction remained anodically controlled for both the Al-11Mo (Fig. 8) and Al-18Mo (Fig. 9) alloys after heat treatment. Referring to Table 2, although some of the Al-11Mo and Al-18Mo alloys precipitated during heat treatment, they still exhibited passive polarization response and the galvanic diagrams predicts the corrosion will be controlled by the anodic dissolution of metal. Only after heat treating

the Al-11Mo to 500°C for 8 h was control for the galvanic reaction changed from anodic (Al passivation) to cathodic (oxygen reduction on Gr fibers).

To confirm the predictions made using the galvanic diagrams, long term galvanic current tests were conducted on sputtered Al, Al-11Mo, Al-18Mo, Al-23Mo, and ternary Al-12Mg-13Mo in the as-deposited condition by coupling the alloy to P75 Gr fibers (Figure 10). Galvanic currents values are equivalent to current densities since the anode areas were 1 cm^2. For all the alloys, the galvanic current initially starts off at relatively high values between 3 and 30 $\mu A \cdot cm^{-2}$, but quickly drops to a low steady state value. The Al-18Mo and Al-23Mo reached low measured galvanic current densities of ~0.04 and ~0.08 $\mu A \cdot cm^{-2}$, respectively which were up to three orders of magnitude lower than the galvanic current density values of 30 $\mu A \cdot cm^{-2}$ measured for pure sputtered Al. Current density of the Al-18 Mo after heat treatment at 400°C for 2 h were comparable to the as-sputtered value of 0.08 $\mu A \cdot cm^{-2}$. Even after heat treatment at 500°C for 2 h the galvanic current density was an order of magnitude lower than for pure sputtered Al. After galvanic testing of seven days (605 ks) the pure sputtered Al had completely dissolved from the Si wafer whereas the Al-Mo alloys remained intact and highly specular.

The Al-12Mg-13Mo alloy exhibited a galvanic current value of 10 $\mu A \cdot cm^{-2}$ which is greater than the binary Al-Mo alloys but still 3 times lower than for pure Al. However, in less than 12 h (40 ks) after immersion in the 0.1 M NaCl, pH 8, solution, the Al-Mg-Mo alloys coupled to P75 Gr fibers had exfoliated and completely lifted away from the sapphire wafer. Due to the short time in solution for the Al-12Mg-13Mo alloy, data for this alloys is not included in Figure 10.

4.0 DISCUSSION

XRD examination indicated that the Al-Mo alloys containing more than 11 atomic percent Mo were amorphous even though the substrate was allowed to heat to approximately 100°C during the sputtering process. The broad peak at 21° was attributed to short range order associated with the Al_xMo_y intermetallic compounds which have high intensity peaks at these low angles. Similarly, the broad peak at 41° was indexed to amorphous Al and is indicative of what has been found for other sputtered and rapidly solidified Al alloys [Ref 13-15]. XRD indicated Mo had not precipitated to form Al_xMo_y intermetallic compounds and thus was available for incorporation into the passive film. Alloys that did not form precipitates during heat treatment exhibited E_{oc} and E_b values very similar to the as-deposited alloys; whereas E_{oc} remained similar to the as-deposited alloys but E_b was more electrochemically

active for heat treatments which produced precipitates. For the Al-18Mo alloy, a noble breakdown potential of approximately 400 mV_{SCE} was observed after heat treatment to 500°C for 2 h even though XRD indicated secondary phases had precipitated.

Galvanic corrosion for all of the as-deposited Al-Mo alloys was controlled by the anodic reaction as indicated by the intersection of the passive region of the anodic curve with the oxygen reduction portion of the P75 cathodic curve. The galvanic diagrams showed that galvanic corrosion of pure Al and 6061 Al alloy were cathodically controlled whereas the galvanic corrosion of the non-equilibrium alloys is anodically controlled. For anodic controlled reactions, corrosion is controlled by ingress of oxygen through the passive film for subsequent reaction with the alloy. Whereas for cathodic controlled corrosion, dissolution of the alloy will occur at a high rate corresponding to the rate of the reduction reaction. The result is the non-equilibrium alloys corrode at a rate about two orders of magnitude lower than pure aluminum of conventional aluminum alloys when galvanically coupled to graphite fibers. Because E_b for the anodic reaction is more noble than the E_{oc} for the cathodic reaction, Al-Mo alloys coupled to Gr fibers are expected to be stable regardless of the area ratios. Decreasing the anode area (or conversely increasing the cathode area) generally results in lateral displacement of the polarization curves, and the corrosion reaction remains anodically controlled. This is beneficial because the composite corrosion behavior will not be adversely affected by increasing the Gr fiber volume.

Even after heat treatment, the binary Al-Mo alloys exhibited high E_{oc} of -550 mV_{SCE}, and a E_b of between 100 and 400 mV_{SCE}. As a result, the galvanic diagrams indicate the couple is anodic controlled and the current density is >1 $\mu A \cdot cm^{-2}$.

Hihara measured the cathodic reaction of P100 Gr, SiC and, TiB_2 in an aerated 3.15 weight percent (0.55 M) NaCl solution [Ref. 3]. Superimposing these results onto the galvanic diagrams presented in this paper shows that the cathodic reaction on the P100 Gr fibers in a higher chloride concentration solution was very similar to the P75 Gr fiber cathodic reaction in 0.1M NaCl, pH 8 (Fig. 11). The open circuit potentials for both P75 and P100 Gr fibers were approximately 0 mV_{SCE}. Figure 11 shows that the Al-Mo alloys would also be galvanically stable with higher modulus Gr fibers such as P100, as well as other reinforcements such as silicon carbide (SiC) and with fiber coatings such as titanium diboride TiB_2. This result is significant because it is the first time that corrosion of Gr reinforced composites has been shown to be controlled by the alloy matrix rather than driven by the Gr fibers.

5.0 CONCLUSIONS

Non-equilibrium Al-Mo alloys fabricated by magnetron sputtering have clearly been shown to be promising matrix alloys for Gr/Al composites. Al with 18 to 23 atomic percent Mo could be heat treated up to 400°C for 8 h without detectable precipitation or change in corrosion behavior. In addition, the Al-23Mo could be heat treated to 600°C for 2 h without degrading the corrosion performance. Al-18Mo heat treated at 400°C for 8 h exhibited an open circuit potential of -556 mV_{SCE}, a breakdown potential of 335 mV_{SCE} and passive current density of ~0.4 $\mu A \cdot cm^{-2}$ in a 0.1 M NaCl, pH 8 solution. These values are very similar to the as-sputtered Al-18Mo alloys and are a significant improvement over pure both pure Al or 6061 Al alloy which are typical matrix materials for Gr/Al composites. Galvanic current densities measured for Al-18Mo and Al-23 Mo of ~0.04 to ~0.08 $\mu A \cdot cm^{-2}$ were 3 orders of magnitude lower than the 30 $\mu A \cdot cm^{-2}$ measured for pure Al in the 0.1 M NaCl, pH 8 solution when coupled to P75 Gr fibers. Galvanic diagrams of the anodic response of the alloy superimposed with the cathodic curve for the P75 Gr fibers predicted the galvanic corrosion rate to be controlled by the rate of the anodic reaction and the Al-Mo alloys will be electrochemically stable when coupled to Gr fibers regardless of the area ratios (in a 0.1M NaCl electrolyte). Galvanic current density values for Al-18Mo alloy heat treated at 400°C for 2h were similar in magnitude to the as-sputtered alloy but began to increased after the 500°C, 2 h treatment.

The ternary Al-12Mg-13Mo alloy also exhibited improved polarization behavior with respect to pure Al and 6061 Al and are a lower density than the Al-Mo alloys. Unfortunately, the ternary alloys exhibited much higher galvanic current density values (~10 $\mu A \cdot cm^{-2}$) and were found to precipitate during heat treatment at the shortest time of 1 h and lower temperature of 400°C which resulted in a loss of passivation.

The polarization and galvanic data indicate that Al alloyed with between 10 and 26 atomic percent Mo provides a matrix that can be processed and consolidated at high temperatures and still retain its inherent corrosion resistance when coupled to the Gr fibers in the composite. Therefore, the optimum alloy composition was determined to be Al-18Mo because it was the lowest density alloy that could be coupled to Gr fibers after heat treatment and retain its passive behavior, and not increase its galvanic corrosion.

ACKNOWLEDGMENTS

The authors would like to gratefully thank John Sedriks for his support. This work was sponsored by the Office of Naval Research under grant N00014-91-J-1196.

REFERENCES

1. L.H. Hihara, Corrosion of Aluminum-Matrix Composites, Ph.D. Dissertation, Massachusetts Institute of Technology, (1985).

2. L.H. Hihara and R.M. Latanision, "Localized Corrosion Induced in Graphite/Aluminum Metal-Matrix Composites by Residual Microstructural Chloride," Corrosion, 1991, vol. 47, pp. 335-340.

3. L.H. Hihara and R.M. Latanision, "Galvanic Corrosion of Aluminum-Matrix Composites," Corrosion, 1992, vol. 48, pp. 546-552.

4. W.C. Harrigan and R.H. Flowers, "Graphite-Metal Composites: Titanium-Boron Vapor Deposit Method of Manufacture," Failure Modes in Composites IV, J.A. Cornie and F.W. Crossman, eds., The Minerals, Metals, and Materials Society, Warrendale, PA, 1977, pp. 319-335.

5. J.H. Payer and P.G. Sullivan, "Corrosion Protection Methods for Graphite Fiber Reinforced Aluminum Alloys," Bicentennial of Materials, Society for the Advancement of Material and Process Engineering, Azusa, CA, 1976 vol. 8, pp. 343-352.

6. V.C. Nardone and J.R. Strife, "Advanced Gr/Mg Composite Development," United Technologies Research Center, Interim Report R89-917711-4, East Hartford, CT, July 1989.

7. W.C. Moshier, G.D. Davis, J.S. Ahearn, and H.F. Hough, "Influence of Molybdenum on the Pitting Corrosion of Aluminum Films," Journal of the Electrochemical Society, 1986, vol. 133, pp. 1063-1064.

8. W.C. Moshier, G.D. Davis, J.S. Ahearn, and H.F. Hough, "Corrosion Behavior of Aluminum-Moybdenum Alloys in Chloride Solutions," Journal of the Electrochemical Society, 1987, vol. 134, pp. 2677-2684.

9. G.S. Frankel, M.A. Russak, C.V. Jahnes, M. Mirzamaani, and V.A. Brusic, "Pitting of Sputtered Aluminum Alloy Thin Films," Journal of the Electrochemical Society, 1989, vol. 136, pp. 1243-1244.

10. G.D. Davis, W.C. Moshier, T.L. Fritz, and G.O. Cote, "Evolution of the Chemistry of Passive Films of Sputter-Deposited, Supersaturated Al Alloys," Journal of the Electrochemical Society, 1990, vol. 137, pp. 422.

11. T.R. Schrecengost, B.A. Shaw, R.G. Wendt, and W.C. Moshier, "Nonequilibrium Alloying for Improving the Corrosion Resistance of Graphite Reinforced Al Metal Matrix Composites," Accepted by Corrosion.

12. D.A. Jones, Principles and Prevention of Corrosion, 1st. ed., Macmillian Publishing Co, New York, NY, 1992, pp. 176-188.

13. P. Furrer and H. Warlimont, "Crystalline and Amorphous Structures of Rapidly Solidified Al-Cr Alloys," Materials Science and Engineering, 1977, vol. 28, pp. 127-137.

14. K. Asami, H. Yoshioka, K. Hashimoto, K. Shimizu and K. Kobayashi, "Superlattice-Like Structure of Sputter-Deposited Amorphous Aluminum-Heavy Element Alloys," Journal of Non-Crystalline Solids, 1989, vol. 110, pp. 258-264.

15. Y. He, S.J. Poon, and G.J. Shiflet, "Synthesis and Properties of Metallic Glasses That Contain Aluminum," Science, 1988, vol. 241, pp. 1640-1642.

Table 1. Alloy Composition and Anodic Polarization Data in 0.1 M NaCl (pH=8) for Binary Al-Mo and Ternary Al-Mg-Mo Non-Equilibrium Alloys.

Alloy Composition (At. %)	E_{oc} (mV vs. SCE)	E_b (mV vs. SCE)	i_{pass} ($\mu A/cm^2$)
Al	-1093	-690	0.10
	-1224	-689	0.70
Al-12Mo	-550	525	6.50
Al-26Mo	-440	750	3.00
	-427	700	0.60
	-460	600	0.80
	-495	770	1.90
	-540	760	4.17
Al-19Mo	-490	320	1.26
	-545	470	1.26
Al-11Mo	-581	220	2.69
	-629	100	23.7†
	-681	0	46.6†
Al-18Mo	-520	461	0.89
	-601	391	3.5
	-555	456	3.63
Al-23Mo	-582	563	45.6
	-582	492	7.60
	-591	496	7.60
Al-12Mg-13Mo	-513	55	1.00
	-573	85	4.50
	-550	39	5.60
Al-11Mg-10Mo	-555	*	*
	-494	*	*
	-542	*	*

† Alloy Started to Passivate, but then Rose to Higher Current Density Before Passivating

* Did Not Passivate

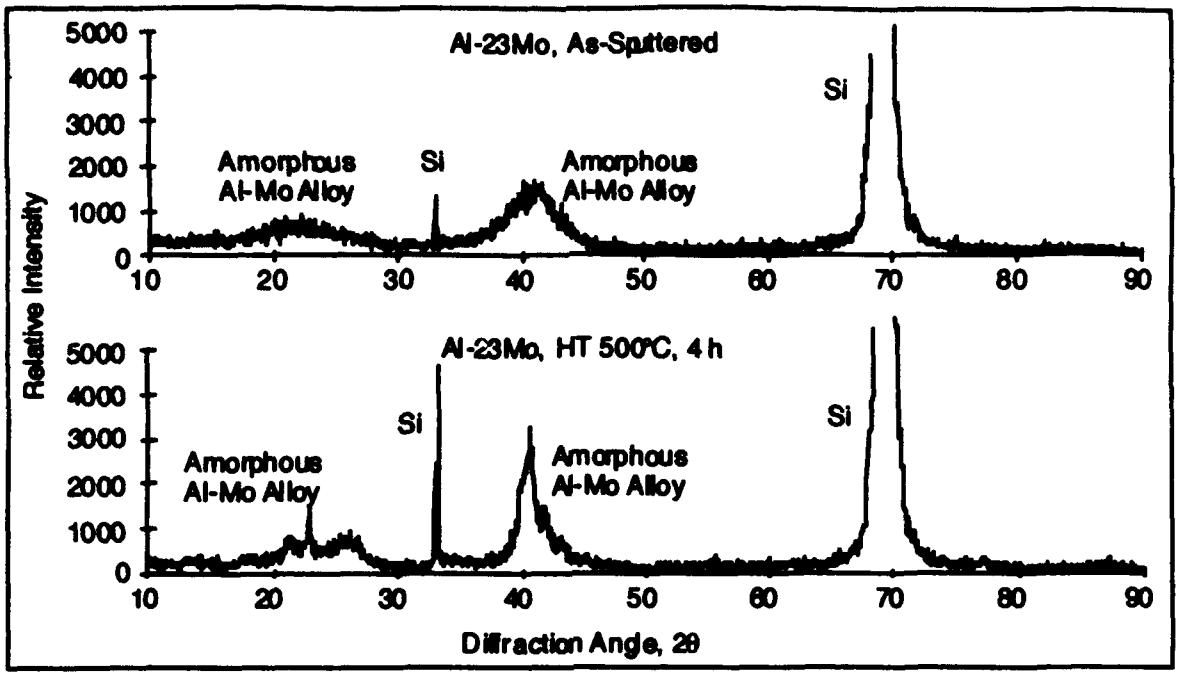

Figure 1. X-ray Diffraction of Al-23Mo Alloy in the As-Sputtered Condition and After Heat Treatment. As-Sputtered, the alloy is amorphous and it is just beginning to precipitate after heat treatment at 500°C for 2 h.

Table 2. Summary of Al-Mo Alloy Structure as a Function of Heat Treatment Time and Temperature.

Heat Treatment Time (h) \ Heat Treatment Temperature	400°C	500°C	600°C
1	Al-11Mo, ppt Al-18Mo, Amorphous Al-23Mo, Amorphous	Al-11Mo, ppt Al-18Mo, ppt Al-23Mo, Amorphous	Al-11Mo, ppt Al-18Mo, ppt Al-23Mo, Amorphous
2	Al-11Mo, ppt Al-18Mo, Amorphous Al-23Mo, Amorphous	Al-11Mo, ppt Al-18Mo, ppt Al-23Mo, Amorphous	Al-11Mo, ppt Al-18Mo, ppt Al-23Mo, Amorphous
8	Al-11Mo, ppt Al-18Mo, Amorphous Al-23Mo, Amorphous	Al-11Mo, ppt Al-18Mo, ppt Al-23Mo, Amorphous	Al-11Mo, ppt Al-18Mo, ppt Al-23Mo, ppt

ppt - fully precipitated

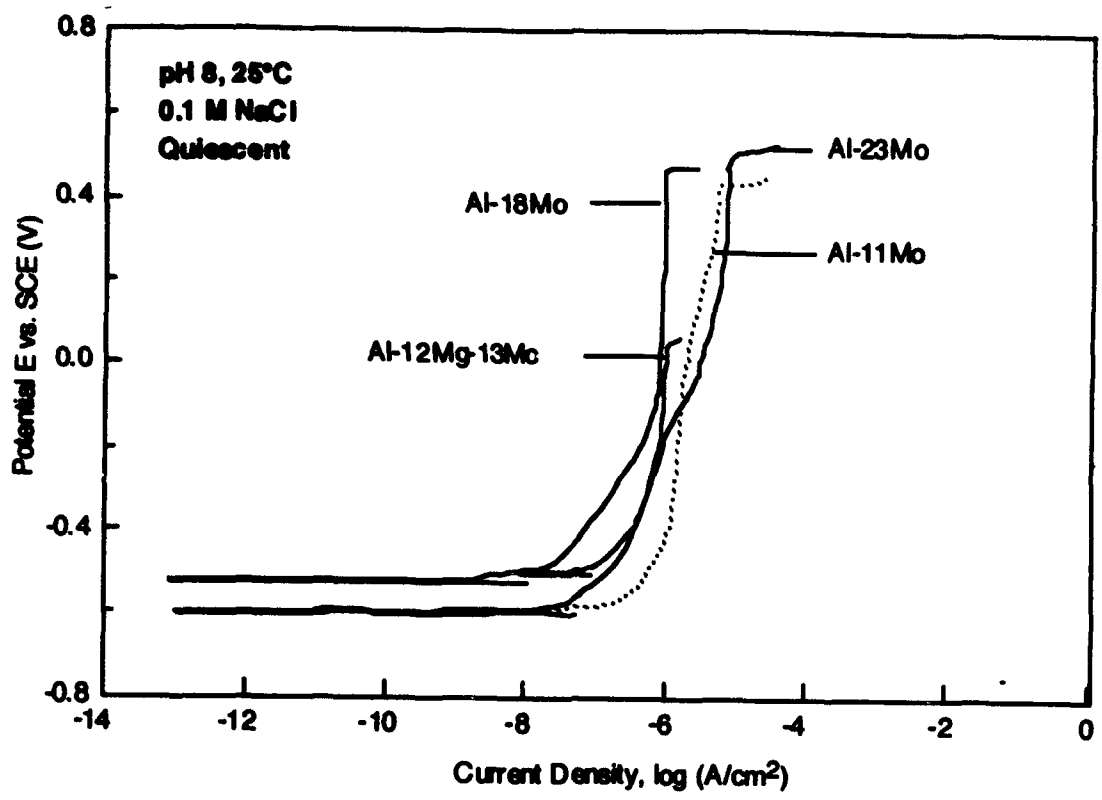

Figure 2. Anodic Polarization Response of Various Al-Mo Alloys, Polarized in Quiescent 0.1M NaCl, pH 8, 25°C.

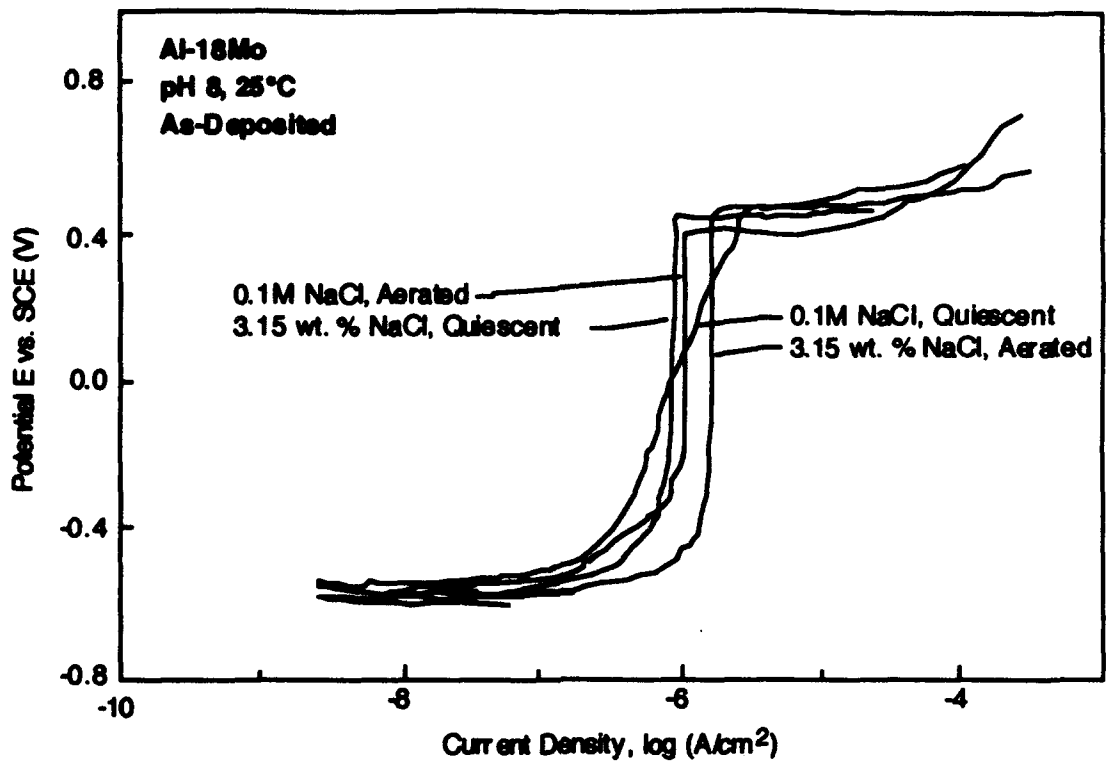

Figure 3. Anodic Polarization Response of Al-18 Mo Used for Detailed Heat Treatment Studies, Polarized in Quiescent and Aerated 0.1M and 3.15 wt. % (0.55M) NaCl, pH 8, 25°C.

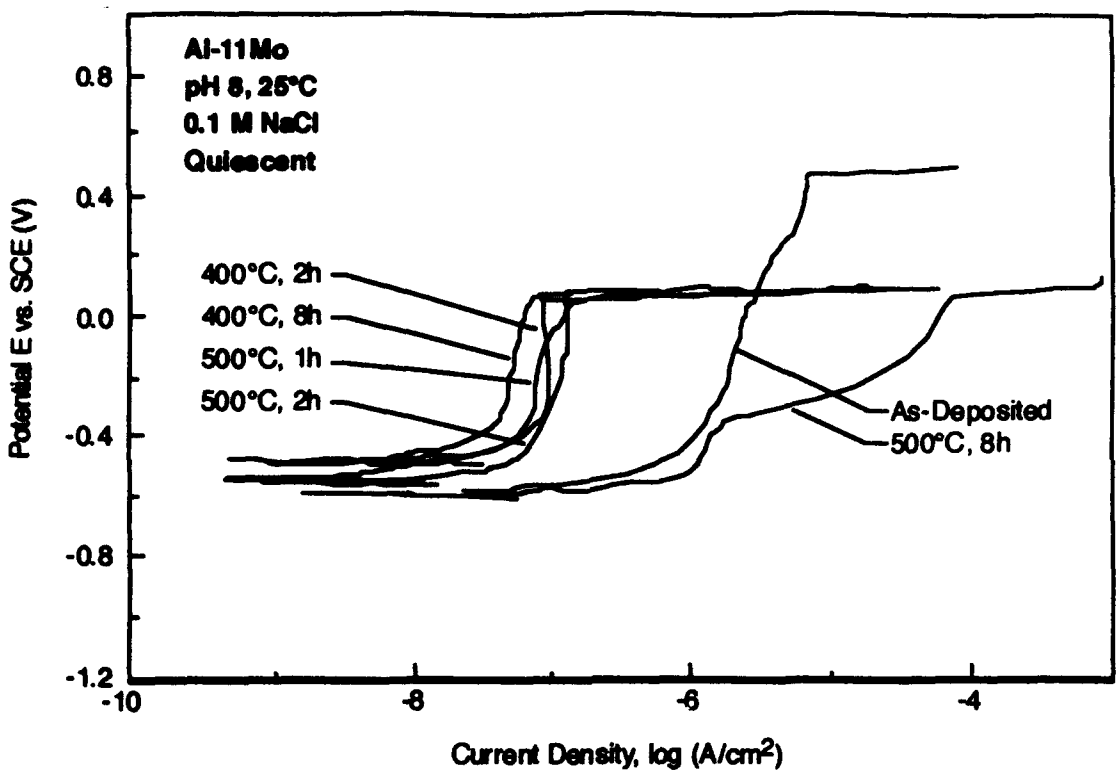

Figure 4. Anodic Polarization Response of Al-11Mo Alloy Before and After Heat Treatment at 400°C for 1 and 2 h and 500°C for 1, 2, and 8 h, Polarized in Quiescent 0.1 M NaCl, pH 8, 25°C.

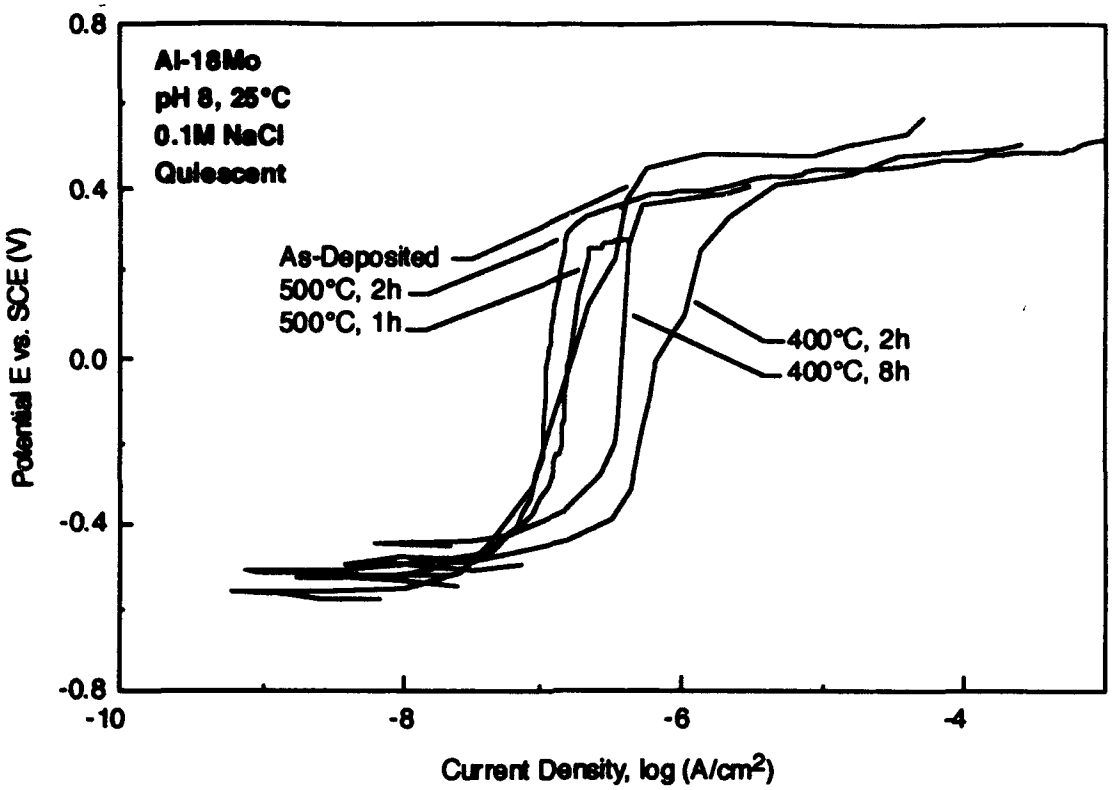

Figure 5. Anodic Polarization Response of Al-18Mo Alloy Before and After Heat Treatment at 400°C for 2 and 8 h and 500°C for 1 and 2 h, Polarized in Quiescent 0.1 M NaCl, pH 8, 25°C.

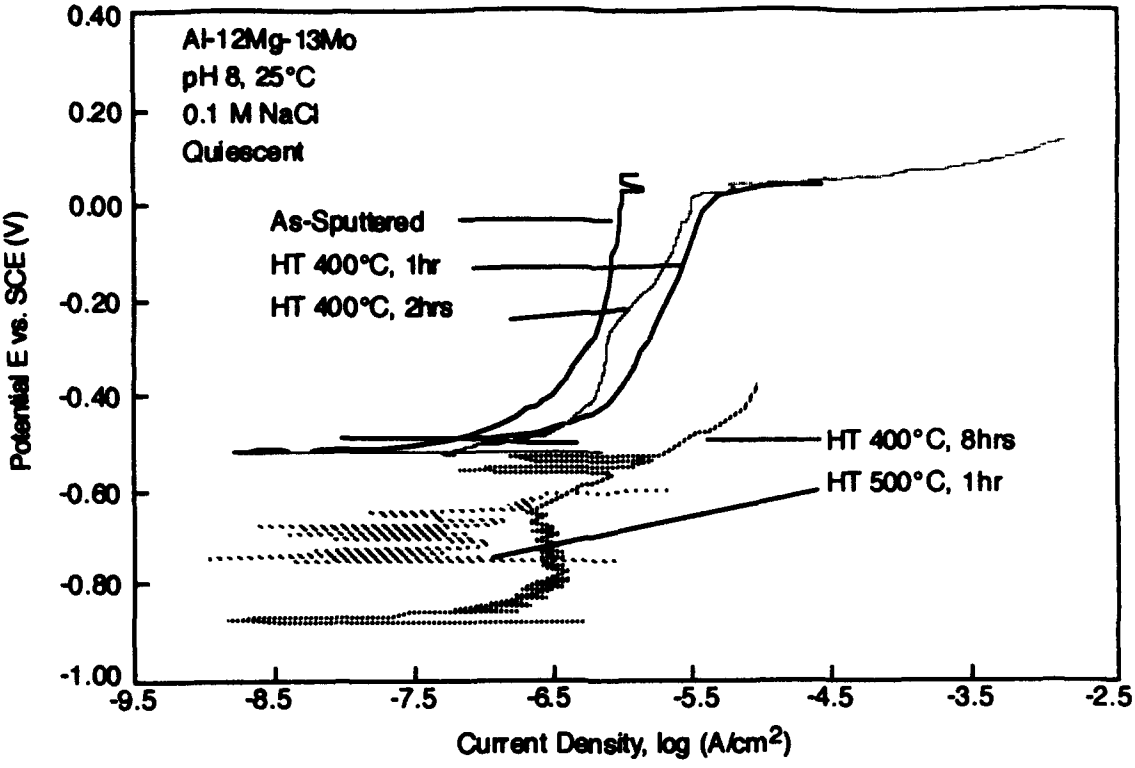

Figure 6. Anodic Polarization Response of Al-12Mg-13Mo Before and After Heat Treatment at 400°C for 1, 2 and 8 hrs and 500°C for 1 hr, Polarized in Quiescent 0.1M NaCl, pH 8, 25°C.

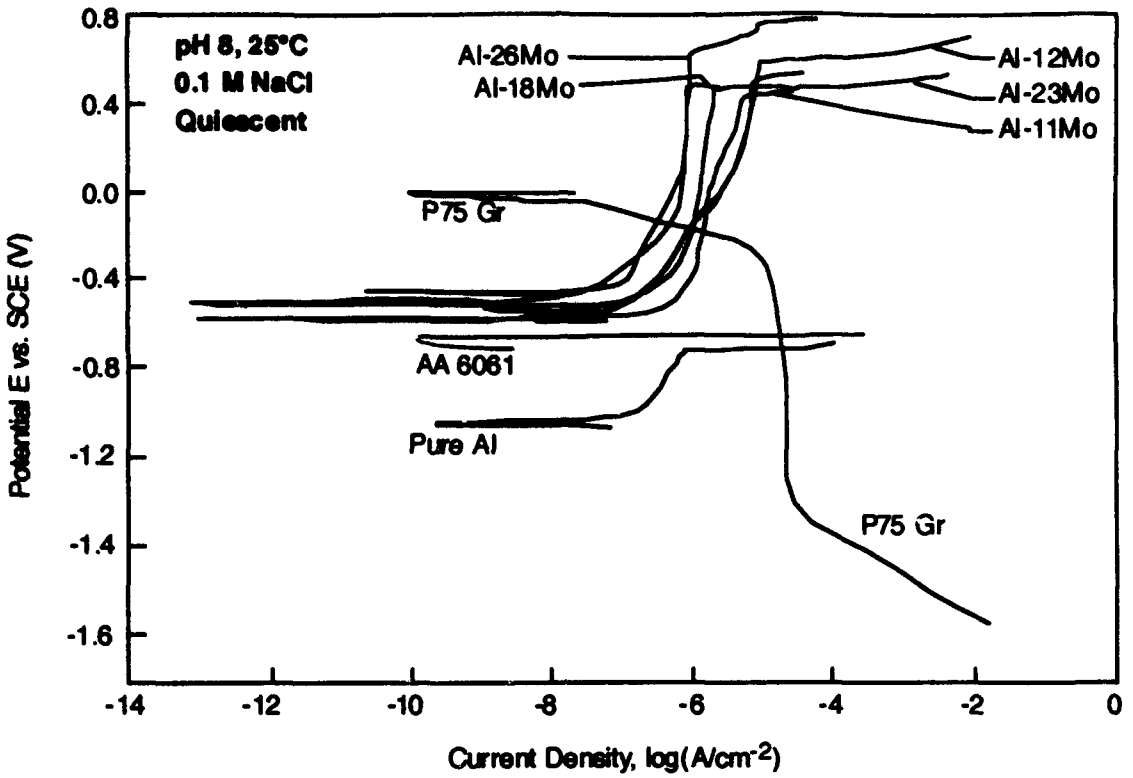

Figure 7. Galvanic Diagram with Anodic Curve of Pure Sputtered Aluminum, Wrought 6061 Al, and Various Sputtered Al-Mo Alloys Combined with the Cathodic Curve for and Equal Area of P75 Graphite Fibers, Tested in Quiescent, 0.1M NaCl, pH 8, 25°C.

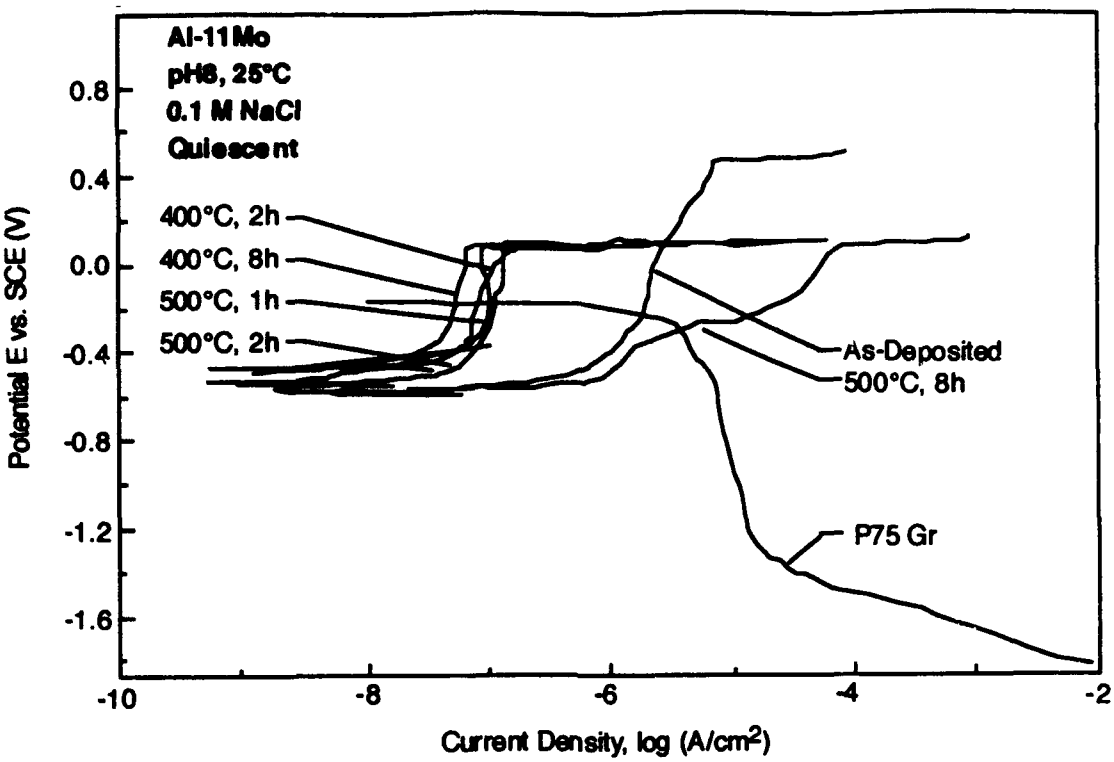

Figure 8. Galvanic Diagram for Equal Areas Al-11Mo Alloy Before and After Heat Treatment at 400° for 2 and 8 h and 500°C for 1, 2, and 8 h With P75 Gr Fibers, Tested in Quiescent 0.1 M NaCl, pH 8, 25°C.

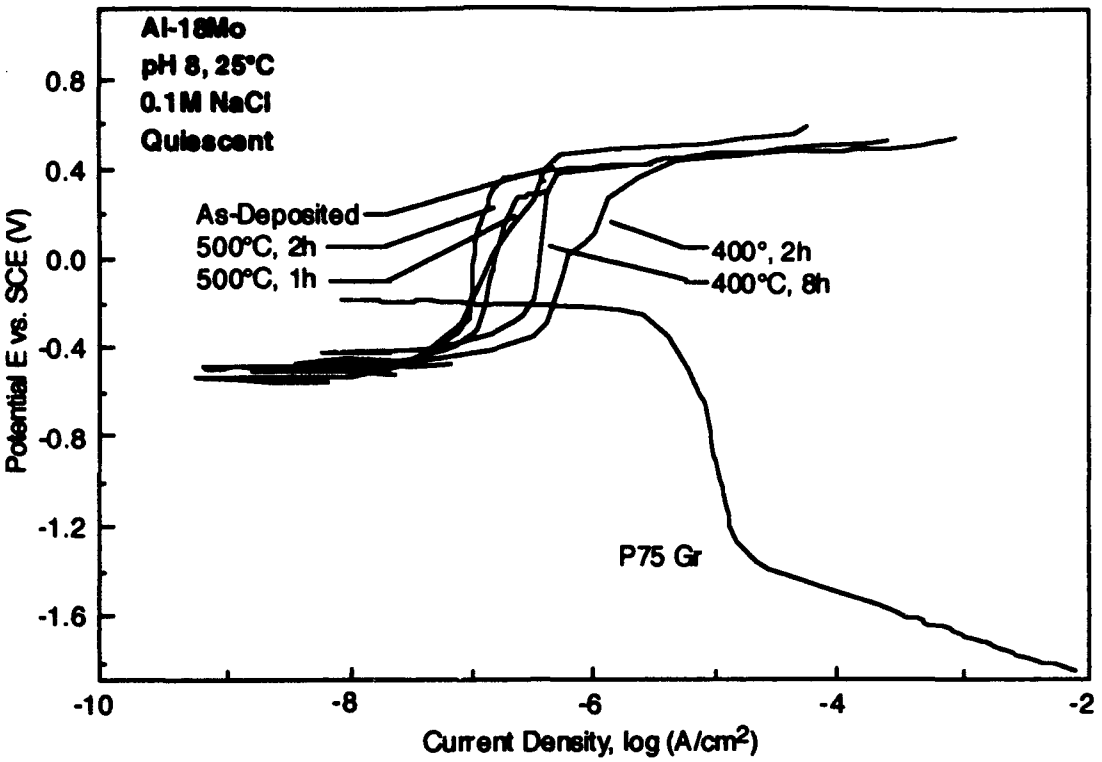

Figure 9. Galvanic Diagram for Equal Areas Al-18Mo Alloy Before and After Heat Treatment at 400°C for 2 and 8 h and 500°C for 1 and 2 h With P75 Gr Fibers, Tested in Quiescent 0.1 M NaCl, pH 8, 25°C.

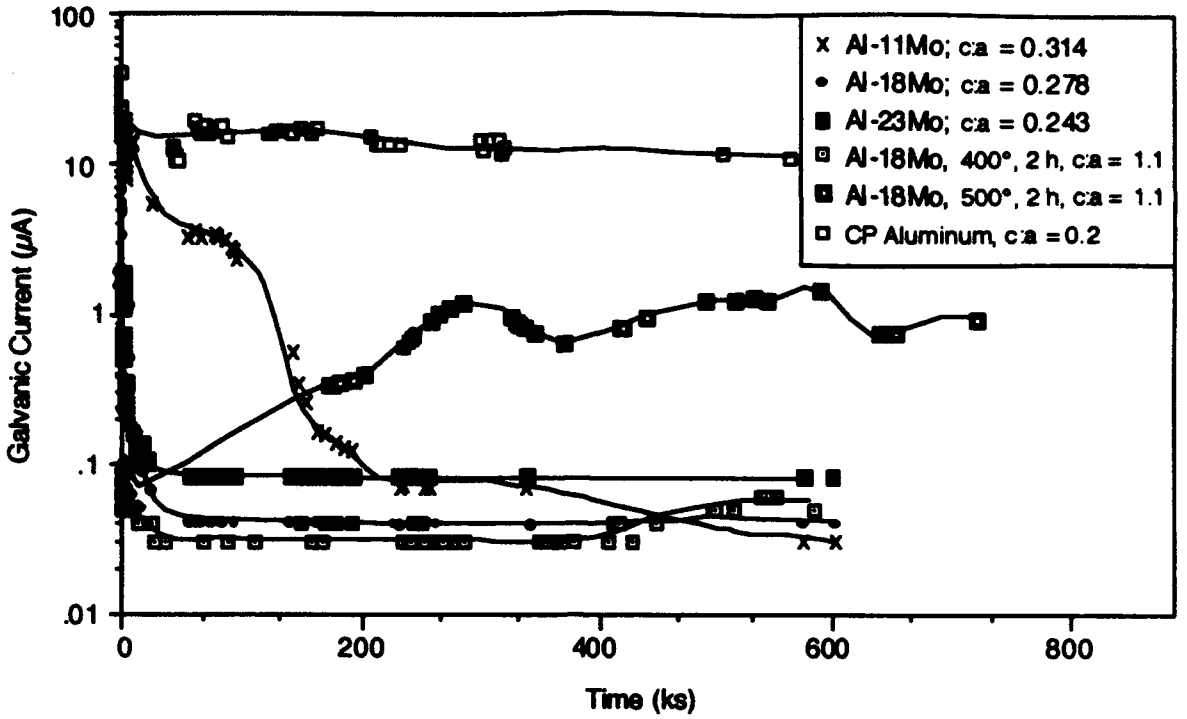

Figure 10. Galvanic Current for Commercially Pure Aluminum and Al-18Mo Alloys (As-Deposited and Heat Treated) Coupled to P75 Graphite Fibers in Quiescent 0.1M NaCl, pH 8, 25°C.

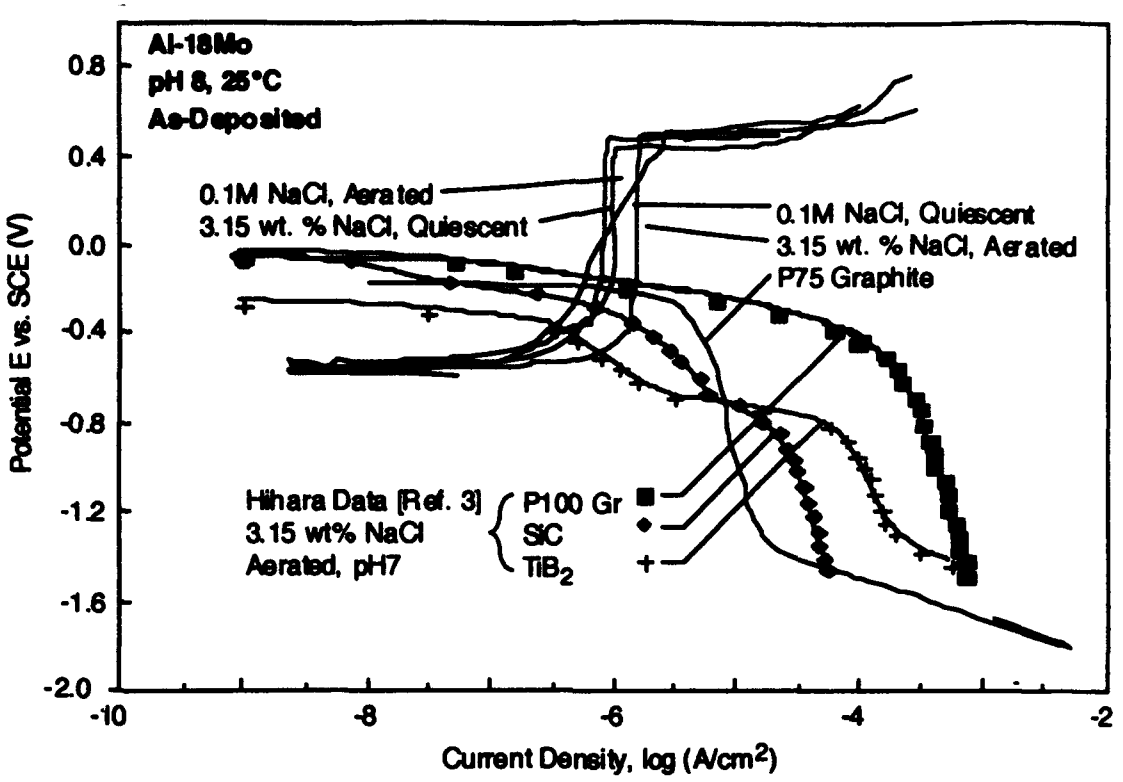

Figure 11. Anodic Polarization Response of Al-18Mo Tested in Quiescent 0.1M and 0.55 M NaCl, pH 8, 25°C Superimposed with P75 Cathodic Curve and P100, SiC and TiB_2 Cathodic Data from Hihara and Latanision [Ref. 3].